AUTHOR'S RESPONSE TO EDITOR'S REVIEW

Manuscript: egusphere-2025-1776

We thank the editor and the two reviewers for their careful reading and constructive suggestions. The revision clarifies methods, corrects processing issues affecting low-signal periods, and documents all screening and trend procedures at the code level. The main physical conclusions are unchanged. The analysis is now more transparent, reproducible, and all affected figures, captions and line-referenced methods have been updated.

We identified and removed a duplicate truncation correction that had been inadvertently applied to the nephelometer scattering coefficients; reprocessing reduces near-zero artefacts and all affected figures and tables were regenerated. The cross-instrument AE33–MAAP comparison is now fully specified with explicit thresholds and clear explanation of the underlying code. The AE33–MAAP screening and fit criteria are instrument-agnostic. We apply uniform detection limits of 0.05 Mm^{-1} to both AE33 (660 nm) and MAAP (637 nm), use a five-sample stuck-value filter for each instrument, and enforce a simple agreement rule: we keep only pairs where neither instrument exceeds the other by a factor of five. Using an ordinary least-squares fit with an intercept, the updated relationship has $R^2 = 0.96$ (Figure R1).

In addition, Figures 1 and 2 were redrawn for clarity as per the editor's comments. Individual responses to the reviewers' comments have been provided below.

Response to Reviewer 1

General comments: This study examines the long-term variability of aerosol optical properties in a boreal forest, categorised by size range. It focuses particularly on the contribution of particles larger than 10 μm, which are usually not considered in aerosol studies as this is the inlet cut-off point. As aerosol optical properties directly influence their radiative effect and larger diameter particles contribute significantly to the AOD, this topic is of great interest for climate modelling parameterisation. Using absorption and scattering measurements coupled with an impactor, the authors investigated the relative contribution of each PM size range to extensive and intensive scattering and absorption parameters. This study's novelty lies in its use of an aerosol classification for PM10, highlighting the significant impact of episodic events such as pollen and dust on optical properties and PM mass. The conclusions provide clear evidence of shifts in the size distribution and composition of aerosols, as well as their seasonality, which are linked to anthropogenic and biogenic emissions. The manuscript is well written and structured. However, several passages are redundant (e.g. the enhanced contribution of dust to the increasing SAE in sections 3.3.2 and 3.3.3), as are some details on the classification matrix (see specific comments). This paper would benefit from being shortened slightly. More importantly, the correction for multiple scattering on the instrument measuring absorption (AE33) was not properly discussed, as it appears to be misunderstood. This is important because it could also explain some discontinuities in the time series from 2018. I consider the manuscript to be publishable after minor revisions and responses to the following points.

Response: Thank you for taking out the time to review our manuscript in such detail. As a general remark, we have now revised the whole manuscript to avoid redundancies. As you had rightly pointed out, the multiple scattering correction factor for the AE31/33 was not properly discussed, which has been addressed now. In fact, a lot of the discontinuities post-2018, actually arose from the truncation correction, being doubly applied to the data of the light scattering coeffcients. This issue has also been corrected and we hope that the revised manuscript addresses all the comments that you have raised.

Comment l.139: Are you sure that the AE33 adjusts the Cref value taking into account aerosol concentrations and environmental conditions? The C value is fixed in the instrument settings, adjustable by the user, and depends on filter material and type.

Response: As outlined in the AE33 manual, the multiple-scattering correction factor (C_{ref}) is fixed in the instrument settings and must be defined by the user. It is determined by the instrument configuration—particularly the filter tape—and does not adjust automatically to ambient conditions. For consistency, we used two fixed, filter-specific values: C_{ref} = 1.57 for 2010–2017 (AE31 with M8020; Luoma et al., 2019) and C_{ref} = 1.39 for 2018–2022 (AE33 with M8060). Yus-Díez et al. (2021) report that the C_{ref} can increase with SSA, but we did not implement environment-dependent adjustments; our choice follows manufacturer guidelines and reflects only the filter properties.

Comment l.356–363: If the absorption coefficient decrease is statistically significant, why are absorbing aerosols less present than in 2010? Are instrumental differences a major contributor?

Response: The absorbing aerosols are "less present" than in 2010 because the fine fraction—which dominates light absorption—has declined. At SMEAR II, $\sigma_{abs,520}$ decreases significantly for PM_{10} (-0.11 ± 0.03 Mm^{-1} yr^{-1}; -8.75 ± 2.11 % yr^{-1}; Fig. S1b; Table S3b) and PM_1 (-0.09 ± 0.02 Mm^{-1} yr^{-1}; -8.87 ± 2.18 % yr^{-1}; Fig. S2b; Table S4b). The similar relative declines indicate that the PM_{10} decrease is likely dominated by its PM_1 (fine-mode) contribution at 520 nm. This is consistent with documented Europe-wide reductions in black-carbon emissions and long-term declines in aerosol absorption over the last decade (Collaud Coen et al., 2020; Yttri et al., 2021). We do not infer a robust long-term decrease for the coarse fraction (PM_{1-10}): its σ_{abs},520 trend is negative but not statistically significant, which is compatible with the episodic, weakly absorbing nature of mineral and biological coarse particles at the site.

Instrumental differences are unlikely to be a major contributor. All absorption data were processed in a harmonized pipeline across the AE31-AE33 transition, including fixed multiple-scattering and filter-loading corrections appropriate to instrument/filter configuration, MAAP intercomparisons where applicable, and uniform QA/QC and completeness criteria (see Methods). Three checks argue against an instrumental origin: (i) no step change is observed at the 2018 transition; (ii) the negative trends persist within each instrument period when analyzed separately; and (iii) the physical seasonality (winter maxima, late-spring minimum) is stable through the record. While small biases associated with filter media and algorithms are possible in principle (Collaud Coen et al., 2010; Zotter et al., 2017), sensitivity tests using plausible parameter choices do not alter

the sign or the significance of the PM_{10}/PM_1 trends. Thus, the observed declines are best explained by real source-side reductions in absorbing aerosols rather than by instrumental artefacts.

Comment l.398: AE33 uses a constant, tape-dependent Cref, but Yus-Díez et al. (2021) showed C also depends on site SSA. Was the AE33 Cref appropriate?

Response: AE33 does not adjust Cref during operation, so we used fixed tape-specific constants: Cref = 1.57 (AE31, M8020, 2010–2017; Luoma et al., 2019) and Cref = 1.39 (AE33, M8060, 2018–2022). Monthly σabs,520 boxplots for PM10, PM1, and PM1–10 show the same late-spring to mid-summer minimum across 2010–2022 with no seasonal-shape break at 2018. Yus-Díez et al. (2021) showed that higher SSA can increase the effective C; because $\sigma abs,520 \propto 1/Cref$, elevated summer SSA would make a fixed 1.39 slightly overestimate summer σabs,520—reinforcing (not creating) the dip. A constant-Cref sensitivity affects only scale: replacing 1.39 with 1.57 rescales the AE33 segment by $1.39/1.57 \approx 0.885$ (~11.5% lower), which cannot shift the month of the minimum or reverse trend signs. Thus, the selected AE33 value is appropriate and does not explain the decrease (Luoma et al., 2019; Yus-Díez et al., 2021).

Comment Part 3.3.2: Much higher variability of SAE after 2018: is there an abrupt change at one nephelometer wavelength?

Response: The apparent post-2018 increase in $PM_{1–10}$ *SAE* variability was a processing artefact: a duplicate truncation correction had been applied to σ_{sca} at 450, 550 and 700 nm. After reprocessing (single application only), the inflated variability disappears. The remaining variability reflects real shifts in the supermicron size mix (relatively larger particles → lower *SAE*; relatively smaller particles → higher *SAE*). Addressing the second point, no wavelength shows an abrupt change: $PM_{1–10}$ σsca at 450/550/700 nm vary smoothly with non-significant p-values (0.09/0.18/0.34), and PM_1/PM_{10} exhibit similarly smooth behaviour. We updated the processing and regenerated the *SAE* plots accordingly.

Comment l. 486-487: But then if the MSC decreases because of the lower sulfate mass fraction within PM_1, why does the MSC time series has a positive trend ?

Sulfate aerosol particles are highly efficient light scatterers, and a decline in sulfate mass fraction would be expected to reduce MSC_{550}. The earlier positive trend in the MSC_{550} of the PM_1 aerosol particles conflicted with this understanding and indicated an inconsistency in the analysis. This was traced to a truncation error caused by the double application of the truncation correction to the nephelometer wavelengths of 450, 550, and 700 nm. Correcting this error restored the light scattering coefficients at 550 nm ($\sigma_{sca,550}$) used in the calculation of MSC_{550} ($MSC_{550} = \sigma_{sca,550}/PM\ mass$), and the updated MSC_{550} time series now accurately represent monthly medians for the PM_1, PM_{10}, and $PM_{1\text{-}10}$ aerosol particles.

The corrected analysis shows that MSC_{550} for PM_1 exhibits a non-significant trend, consistent with the reduction in sulfate mass fraction and its effect on scattering efficiency (Pandolfi et al., 2014; Seinfeld & Pandis, 2016). MSC_{550} for PM_{10} and $PM_{1\text{-}10}$ are also non-significant, reflecting the stronger contribution of coarse particles in these fractions, whose scattering efficiency is less sensitive to sulfate changes. These results indicate that sulfate

reductions are mainly expressed in PM_1, while the larger size fractions remain buffered by coarse-mode contributions, which dilute the effect of composition on scattering.

The revised MSC_{550} trends are now consistent with the expected effects of sulfate on scattering efficiency across size fractions. The smooth and continuous time series demonstrate that the updated results are free from artefacts and reflect changes in aerosol composition rather than instrumental issues. This correction resolves the earlier inconsistency by linking reductions in sulfate mass fraction directly to the scattering signal in PM_1, clarifying how size-resolved contributions shape MSC_{550} and improving confidence in the interpretation of long-term scattering behavior across all particle size ranges.

Comment from l.398: AE33 still has a constant C_{ref} value, depending on the filter tape. Yus-Diez et al. (2021) have shown that this C value is also depending on the SSA measured at the site. One can wonder whether the C value used in the AE33 was appropriate.

Response: The $\sigma_{abs,520}$ boxplots (Fig. S10) for 2010–2017 and 2018–2022 address whether the seasonal decrease in May–July is consistent across the instrument transition. In both periods, PM_{10}, PM_1, and PM_{1-10} show clear winter maxima and a pronounced May–July reduction, with no evidence of discontinuities. This stability demonstrates that the decrease is a persistent feature of the boreal aerosol cycle rather than an artefact of instrumentation or data processing.

The AE33 multiple-scattering correction factor (C_{ref}) was applied as a fixed, filter-specific constant. We used C_{ref} = 1.57 for 2010–2017 and C_{ref} = 1.39 for 2018–2022, the manufacturer-recommended values for the M8020 and M8060 filter tapes, respectively (Luoma et al., 2019). Yus-Díez et al. (2021) showed that the effective C_{ref} can increase under high-*SSA* (strongly scattering) conditions, but we did not implement such environment-dependent adjustments here. Because C_{ref} is fixed within each period and independent of *SSA*, it cannot account for or influence the May–July decrease in $\sigma_{abs,520}$ observed in either interval.

Comment l. 517-518: The multiple scattering effect on the AE filter would increase if the SSA is higher (which is the case, regarding Fig 4), leading to a higher correction factor C, and to even lower σ_{abs}, so the correction of this parameter can't really explain the decrease of σ_{abs} during May, June and July. Related to that, do these boxplots (Fig 3 and 4) look the same before and after 2018?

Response: For all three size fractions (PM_{10}, PM_1, and PM_{1-10}), the $\sigma_{abs,520}$ boxplots for 2010–2017 and 2018–2022 show similar seasonal patterns, with clear winter maxima and a pronounced reduction in May–July. The magnitude and timing of this decrease arensistent across both time periods, with no evidence of discontinuities or offsets between the datasets. This stability indicates that the observed May–July reduction is a persistent feature of the boreal aerosol annual cycle and is not attributable to the 2018 instrument transition.

The AE33 multiple-scattering correction factor (C_{ref}) was applied as a fixed parameter for each period, determined by the filter type used. For 2010–2017, we retained C_{ref} = 1.57 following Luoma et al. (2019), appropriate for TFE-coated glass fibre filters. For 2018–2022, we used C_{ref} = 1.39, the recommended value for the Magee M8060

filter tape installed in our AE33. These values were not altered based on aerosol concentration or environmental conditions, ensuring consistency and avoiding potential bias in $\sigma_{abs,520}$ trends.

The SSA_{550} boxplots indicate elevated values during May–July for all size fractions, reflecting the stronger contribution of scattering relative to absorption in this period. While higher SSA_{550} can increase the magnitude of the multiple-scattering effect, the fixed C_{ref} values applied in each period mean that this effect does not influence the observed seasonal σabs reduction. The consistency of SSA_{550} patterns before and after 2018 further supports the interpretation that the May–July σ_{abs} decrease reflects atmospheric variability rather than methodological artefacts.

Comment l. 218 and Fig S9: What is the r^2 value of the linear regression? Did you keep all the AE data, even the one that were far from the slope?

Response: R^2 of the AE33–MAAP linear regression is 0.96 using ordinary least squares with an intercept. The fitted relation is $\sigma_{abs,660}$ (AE33) = 2.33 x $\sigma_{abs,637}$ (MAAP) + 0.16 Mm^{-1} (Figure R1). No, we did not keep all aethalometer data, especially those far from the slope. Points were removed automatically if they failed objective screening. We did not hand-pick points.

Previously, in old Fig. S9 (Figure R2), we used asymmetric low-value thresholds: AE33 ≥ 0.0165 Mm^{-1} and MAAP ≥ 0.165 Mm^{-1}, based on early heuristics and mis-specified limits, partly because AE33 read higher than MAAP in time series (Figure R3). We removed only ≥ plateaus of 10 identical data points, applied a one-sided agreement bound, and performed no residual outlier screening. Result: slope 2.36, intercept 0.08, and R^2 = 0.93. These choices had increased the scatter, although not by much.

Now, in revised Figure S9 (Figure R1), we apply a uniform detection limit of 0.05 Mm^{-1} to both instruments, remove ≥ plateaus of 5 identical data points, and enforce a symmetric plausibility check by excluding pairs where one instrument exceeds fivefold over the other, implemented as not (AE33 ≥ 5 x MAAP or MAAP ≥ 5 x AE33).

This revised treatment improves the R^2 from 0.93 to 0.96.

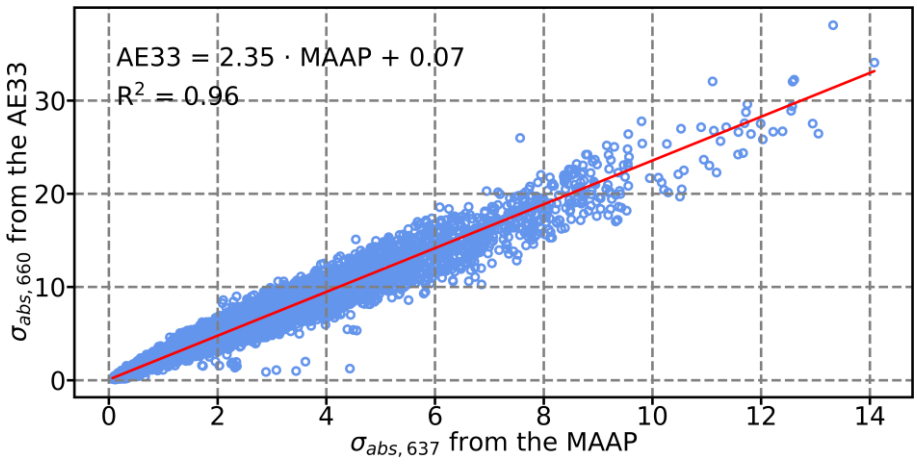

Figure R1. Ordinary least squares regression of $\sigma_{abs,660}$ from the AE33 with respect to $\sigma_{abs,637}$ from the MAAP (New).

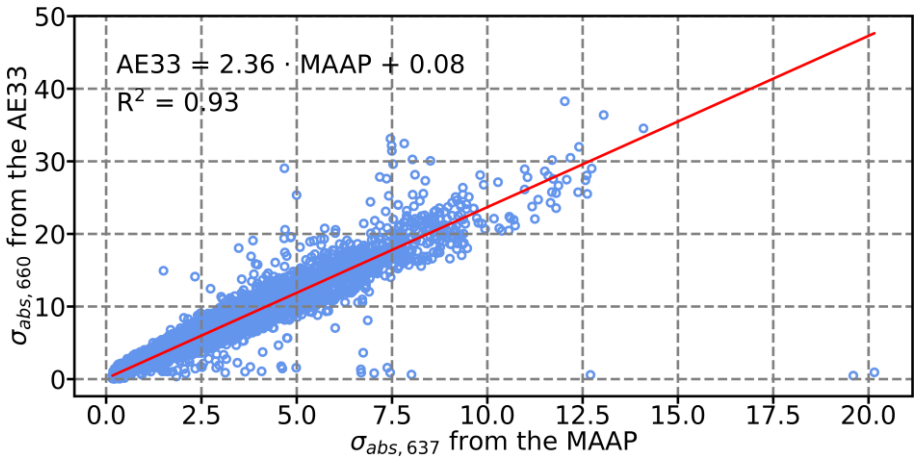

Figure R2. Ordinary least squares regression of $\sigma_{abs,660}$ from the AE33 with respect to $\sigma_{abs,637}$ from the MAAP (Old).

Technical corrections:

l. 89-90 : "two Magee Scientific Aethalometers"

Response: Error fixed

l. 92-93 : please fix the intervals in the parenthesis : "(i.e. ≤ PM1, between PM1 and PM2.5, between PM2.5 and PM10, ≤ PM10, > PM10)".

Response: Fixed.

l. 106 "aethalometers"

Response: Fixed.

l. 127-128 please fix the citation format.

Response: Fixed.

l. 212 please fix the citation format.

Response: Fixed.

l. 269: "which is used in conversion of σ_{abs} to BC mass"

Response: Corrected.

l. 277-278 : The composition is not a physical characteristic

Response: Corrected to “the physicochemical characteristics of aerosols”.

l. 319 : “ contribution additional variability” this sentence is strange

Response: Corrected to “Pollen and dust events (green and red stars; Sect. 2.3) introduce additional short-term variability in the observed optical and mass properties without altering the sign or statistical significance of the long-term trends (Table 3).”

Fig 1 and Fig 2: Please provide the meaning of the blue shaded area on panels a and b.

Response: The legend has been changed.

l. 333 : Please provide at least for the first notification the information on the two different values : slope and relative trend.

Response: This has been done everywhere in the paper now.

l.475 : Why “albeit” ? Statistically significant is not contrasting with the beginning of the sentence.

Response: This section has been changed altogether.

Fig 5 : It would be great to remove the decimal part of the y-axis ticks on panels c and d. Furthermore, it is a bit difficult to see with this representation the contribution of pollen and dust events to Super PM10, as we don’t see on which months occurred these events. Maybe you can add the red and green stars also on panels c and d ?

Response: The decimal part of the y-axis ticks on panels (c) and (d) have been removed. Instead of adding any further information on seasonal variation of dust and pollen events in this paper, we are currently working on a forthcoming manuscript, which delves deeper into the event analysis of dust and pollen events.

Response to Reviewer 2

We want to thank the reviewer for crticicall examining the manuscript. We hope that the responses below address all your concerns.

Comment Line 225: How does autocorrelation in time series data affect the results of the Mann-Kendall test, and how is this addressed?

Response: The classical Mann–Kendall (MK) trend test assumes serial independence. Positive autocorrelation reduces the effective information in a series; if it is not accounted for, the MK variance is underestimated and the

test becomes too liberal (p-values spuriously small). Strong negative autocorrelation has the opposite effect. In other words, persistence can make a weak trend appear "significant" unless the MK variance is adjusted.

We use a variance-corrected MK that replaces the nominal sample size n with an effective sample size,

$$n_{eff} = \frac{n}{1+2\sum \rho_k} \ (\geq 1), \qquad \text{R2}$$

computed from the statistically significant autocorrelation coefficients (ρ_k) of the analysis series. Concretely, our function *effective_sample_size()* evaluates the autocorrelation function (ACF) for lags $k = 1 \ldots n_{lags}$ with $n_{lags} = \min(20, \lfloor n/4 \rfloor)$ (lag 0 excluded), retains only lags with $|\rho_k| > 1.96/\sqrt{n}$, and then forms n_{eff}. This n_{eff} is used inside *modified_mann_kendall_trend()* to compute the MK variance and Z statistic, yielding autocorrelation-aware p-values. Importantly, the trend magnitude is estimated with Theil–Sen and is unchanged by this correction; only the significance is adjusted. We do not prewhiten, thereby avoiding potential slope bias.

(i) Pseudo-daily variables—*PM mass*, MSC_{550}, MAC_{520}: in *plot_trend_ps,eudo_daily()* we

(a) mask day-level outliers using a modified Z-score, that is flag x_i if $|0.6745(x_i - \text{median})/\text{MAD}| > 3.5$,

(b) estimate the slope with Theil–Sen, and

(c) test significance with the effective sample size (ESS)–corrected Mann–Kendall test described above. Any day/interval completeness gates are enforced upstream when the pseudo-daily series are constructed; flagged pollen/dust events are annotated for context but not removed.

(ii) Monthly-median variables—$\sigma_{sca,550}$, $\sigma_{abs,520}$, SSA_{550}, *SAE*, *AAE*: we first form monthly medians only when a month has ≥75%age valid hours (based on the native sampling interval), which reduces short-lag persistence; we then fit Theil–Sen and apply the same ESS-corrected MK to the monthly series.

Across both paths, the slope estimator (Theil–Sen) provides a robust trend magnitude, while the MK p-values are explicitly corrected for autocorrelation. This prevents inflated significance due to persistence and yields a conservative, reproducible assessment of trend detection appropriate for environmental time series.

Comment Line 227: How do seasonal fluctuations and non-linear trends influence the interpretation of long-term aerosol optical trends?

Response: Seasonal patterns can skew how long-term change looks. If the size or timing of the yearly cycle shifts—such as weaker winters, earlier or larger spring pollen or dust peaks, or stronger warm-season SOA with frequent spring–autumn NPF—a straight line through the raw series will absorb that movement. The apparent slope can become too big or too small, and in rare cases flip sign. These patterns also create persistence, so ignoring serial correlation can overstate confidence; our inference targets the slow component and uses statistically robust, dependence-aware trend tools (Mann, 1945; Kendall, 1975; Hamed and Rao, 1998; Yue and Wang, 2004).

Non-linear behavior brings a different challenge. Curvature across years, step changes around instrument transitions, and short pollen or dust episodes split the record into periods that do not behave the same way. One constant slope across the full series then averages dissimilar regimes and can misstate what is happening now,

even when the overall fit appears good. In practice this can bias both the estimated magnitude and its assessed significance, or shift the mean without altering direction. That is why we examine shape and regime changes before summarizing the record with a single tendency. Effects matter for attribution and interpretation.

We reflect those issues in the analysis pipeline. For PM mass, MSC_{550}, and MAC_{520} we build pseudo-daily means by keeping days with ≥18 time-stamped observations, masking outliers with a modified Z-score, and averaging reliably. For the $\sigma_{sca,550}$, $\sigma_{abs,520}$, SSA_{550}, *SAE*, and the *AAE*, we compute monthly medians when a month has ≥75% valid hours, masking monthly outliers. We report the trend using the robust median slope (Theil, 1950; Sen, 1968) and test it with a statistically conservative Mann–Kendall adjusted for autocorrelation by shrinking the effective sample size using significant ACF lags up to *n_lags* = min(20, ⌊n/4⌋) (Hamed and Rao, 1998; Yue and Wang, 2004).

Line 40:"which could explain higher concentrations in winter." Add “higher coarse particle concentrations in winter."

Response: Now, the introduction section has been changed, so this line is redundant.

Line 41-42: "while pollen and spores often originate from more local biogenic emissions that are highly episodic and seasonal." The phrase "more local" can be improved.

Response: Same as above.

Line 43:"Sea salt, though typically associated with marine environments, can occasionally reach boreal forests during strong winds." Could be written as "can occasionally be transported to boreal forests during strong wind events."

Response: Same as above.

Line 45: Replace "over 10 µm" (line 45) with >10 µm for consistency with earlier notation (e.g., line 23: >1 µm).

Response: Corrected.

Line 45–47: "may not be fully captured by standard PM10 measurements, leaving their contributions underrepresented...". Add the reason here “due to cut-off inlets or sampling loss”.

Response: Line changed to, “Coarse-mode aerosol particle sizes span about 1 µm to > 10 µm, so many pollen grains and fungal spores exceed the PM_{10} impactor cut-off and are underrepresented in PM_{10} measurements (Després et al., 2012; Yli-Panula et al., 2009).”

Line 49:"contribute to atmospheric heterogeneity". Specify "spatial and temporal heterogeneity" for more scientific clarity.

Response: Corrected as advised.

Line 51: the reference added here is in non-chronological citation order. Also, Brasseur et al., 2024 is cited in a 2025-dated document. While plausible (if published in early 2024), ensure this reference exists. If not, update to the correct publication year.

Response: I have used a citation manager tool that created citations as per the author's last name. That is why Brasseur appears first. Also, the Brasseur et al. was published in 2024 and the link to the correct paper is included in the reference list.

Line 57:"potentially leaving a significant fraction of aerosol mass unquantified". Replace with "potentially resulting in a significant underestimation of aerosol mass."

Response: Done.

Line 64-68: These line are slightly redundant with earlier statements and too long

Response: This paragraph has been rewritten.

Line 86–87: "Thus, SMEAR II represents the typical conditions that may be found in a boreal forest." Should be replaced by "Therefore, SMEAR II reflects typical boreal forest conditions."

Response: Changed as advised.

Line 88: "It is a part of the European Aerosols, Clouds, and Trace Gases Research Infrastructure or ACTRIS…" should be replaced by "The station is part of ACTRIS (Aerosols, Clouds, and Trace Gases Research Infrastructure)..."

Response: Done.

Line 60: "such as pollen, may escape standard measurements, whereas smaller coarse-mode particles, such as fungal spores and dust, are more likely to be captured. Replace with "Smaller coarse-mode particles like fungal spores and dust are more likely to be captured, whereas larger ones, such as pollen, may escape detection."

Response: Corrected.

Line 77: Define "super-PM_{10}" earlier for clarity:37-48: Provide references for these statements.

Response: Done.

Line 88-93: 4 instruments have been used primarily, but only 3 have been covered here.

Response: Changed.

Line 97: 'a' Dp >10 µm

Response: Done.

Line 104: is aimed 'to' be kept

Response: Corrected.

Line 120: Are there any recent publications post Liousse et al., 1993 which cover this?

Response: Yes and they have been added.

Line 149: Use l min-1 for consistency.

Response: Done.

Line 237-238: This is repetition of 232-233.

Response: Changed.

Line 289: Write PM1–10 with subscript.

Response: Done.

Line 341: SOA already defined in line 33, so expansion is not needed here.

Response: Corrected.

Line 342: Instead of 'biogenic VOC', use BVOC as already defined.

Response: Done.

Line 460: OA has not been defined previously.

Response: This text has been removed.

Line 645: SOA already defined in line 33, so expansion is not needed here.

Response: This text has now been removed altogether.

Line 709: typo after reference link

Response: Changed.

Line 760: Provided link is not working.

Response: Corrected.

Line 927: Link to reference has not been provided. Pls correct all the incorrect references.

Response: The reference has been removed and all the links have now been checked.

Use subscript formatting for PM size ranges (e.g., $PM_{1–10}$ instead of PM1-10).

Response: Fixed everywhere.

Measurement Report: Optical properties of supermicron aerosol particles in a boreal environment

Sujai Banerji[1], Krista Luoma[2], Ilona Ylivinkka[1], Lauri Ahonen[1], Veli-Matti Kerminen[1], and Tuukka Petäjä[1]

[1]Institute for Atmospheric and Earth System Research (INAR)/Physics, Faculty of Science, University of Helsinki, Helsinki, Finland

[2]Finnish Meteorological Institute, Helsinki, Finland

Correspondence to: Sujai Banerji (sujai.banerji@helsinki.fi)

Abstract

Supermicron aerosol particles (PM_{1-10}; here defined as 1 µm < aerodynamic diameter ≤ 10 µm) play a crucial role in aerosol-climate interactions by influencing light scattering and absorption. However, their long-term trends and episodic significance in boreal environments remain insufficiently understood. This study examines measurements of optical properties and mass of PM_{1-10} over a 12-year period at the SMEAR II station in Hyytiälä, Finland, focusing on their variability and key drivers. By assessing long-term trends, seasonality, and episodic variability, the study provides new insights into the role of these particles in aerosol-climate interactions. Episodic events, such as pollen outbreaks and dust transport, are identified as major contributors to PM_{1-10} variability and their role in atmospheric processes. In addition, cascade impactor filters were used to quantify super-PM_{10} particles (D_p > 10 µm), which are not detected by optical instruments, addressing key detection limitations. The findings reveal significant long-term trends and pronounced seasonality in PM_{1-10} mass and optical properties, emphasizing their importance in boreal environments and their episodic relevance in coarse-mode aerosol characterization.

1. Introduction

Aerosols are integral to atmospheric processes, influencing climate, air quality, and radiative forcing. Among them, coarse-mode aerosol particles, which are typically defined as particles with diameters > 1 µm play a significant role in light scattering and absorption, directly impacting radiative forcing. Their size and optical properties make them dominant contributors to aerosol optical depth (AOD), particularly at longer wavelengths. Coarse-mode aerosol particles, such as biological aerosols found in the boreal environment, also contribute to cloud microphysics by serving as ice-nucleating particles (Brasseur et al., 2022). Despite their importance, the optical properties and particulate matter mass (PM mass) of coarse-mode aerosol particles remain understudied (Cappa et al., 2016).

Boreal forests, covering approximately 15% of the Earth's terrestrial surface, represent a unique natural laboratory for studying aerosol-climate interactions in biogenically dominated environments. These ecosystems emit large quantities of biogenic volatile organic compounds (BVOCs); Guenther et al. (2006)), which drive the formation of secondary organic aerosols (SOA), significantly influencing aerosol size distribution and, therefore, light scattering and absorption processes (Petäjä et al., 2022; Tunved et al., 2006). Additionally, episodic events such as pollen outbreaks and long-range transport of mineral dust contribute to aerosol variability in boreal regions (Manninen et al., 2014).

Coarse-mode aerosol particles in boreal environments are emitted predominantly through primary processes rather than formed secondarily, arising from mineral dust, pollen, fungal spores, plant debris, sea salt, and episodic

sources such as wildfires and small-scale wood combustion (Zieger et al., 2015; Yli-Panula et al., 2009; Varga et al., 2023; Andreae and Merlet, 2001; Reid et al., 2005). Wildfires are predominantly a summer phenomenon, whereas small-scale wood combustion peaks in winter and likely explains the higher winter concentrations. Dust commonly reaches Finland via long-range transport, whereas pollen and fungal spores are locally or regionally emitted and highly seasonal (Varga et al., 2023; Yli-Panula et al., 2009). Marine sea-salt intrusions occasionally affect inland boreal forests during strong winds or frontal passages (Zieger et al., 2015; Tunved et al., 2006).

Coarse-mode aerosol particle sizes span about 1 µm to > 10 µm, so many pollen grains and fungal spores exceed the PM_{10} impactor cut-off and are underrepresented in PM_{10} measurements (Després et al., 2012; Yli-Panula et al., 2009). This selectivity can bias coarse-mode analyses during episodic biological events, unless sampling and interpretation account for partial capture or exclusion. Determining whether such particles are sampled is crucial for quantifying impacts on aerosol optical properties, radiative forcing, and aerosol-cloud interactions (Zieger et al., 2015; Tunved et al., 2006). Wildfire smoke produces fine-mode particles but can include coarse fractions from smouldering or resuspension (Andreae and Merlet, 2001; Reid et al., 2005).~~Coarse-mode particles in boreal environments are dominantly primary aerosol particles—particles emitted directly into the atmosphere rather than formed through chemical reactions. These include dust, pollen, fungal spores, plant debris, and sea salt, as well as particles from episodic sources like wildfires or small-scale wood combustion, which could explain higher concentrations in winter. Mineral dust is typically transported long distances, while pollen and spores often originate from more local biogenic emissions that are highly episodic and seasonal. Sea salt, though typically associated with marine environments, can occasionally reach boreal forests during strong winds. Wildfire emissions, though predominantly in the fine mode, can contain coarse-mode particles, particularly in smoldering phases or from ash deposition.~~

~~The size fractions of these coarse-mode particles range from 1 µm to over 10 µm. Pollen grains and larger fungal spores often exceed the PM_{10} cut-off and may not be fully captured by standard PM_{10} measurements, leaving their contributions underrepresented in coarse-mode analyses. Understanding the extent to which these particles are detected or left out of PM_{10} measurements is crucial for characterizing their impacts.~~

The natural components of coarse-mode aerosol particles contribute to spatial and temporal ~~atmospheri~~ heterogeneity, influencing key microphysical processes, such as the activation of ice-nucleating particles (INPs)~~,~~ and playing a vital role in atmospheric processes like cloud formation, nutrient cycling~~,~~ and radiative interactions (Brasseur et al., 2024; Després et al., 2012; Mahowald et al., 2014; Schneider et al., 2021). Despite their recognized importance, the interactions between these natural components and atmospheric dynamics in boreal environments remain poorly characterized, particularly in the context of episodic events like pollen releases, dust transport~~,~~ and potential contributions from biomass burning.

The coarse-mode size range also presents challenges for optical instruments, with upper size cut-offs typically set to 10 µm, potentially resulting in ~~leaving~~ a significant underestimation ~~fraction~~ of aerosol mass ~~unquantified~~ (Zieger et al., 2015). This undetected mass fraction is crucial for achieving optical closure and improving vertical column density estimates in boreal environments. Furthermore, the detection of coarse-mode aerosol particles depends on their size~~:~~ particles ~~>larger than~~ 10 µm, Smaller coarse-mode particles like fungal spores and dust

Formatted: English (United States)

are more likely to be captured, whereas larger ones, such as pollen, may escape detection.~~such as pollen, may escape standard measurements, whereas smaller coarse-mode particles, such as fungal spores and dust, are more likely to be captured.~~

The knowledge gaps regarding coarse-mode aerosol particles hinder our ability to fully understand their optical and mass properties and their contributions to regional and global atmospheric processes. To capture both long-term trends and episodic variability, we analyze the optical properties and PM mass of $PM_{1\text{-}10}$ aerosol particles at the SMEAR II station in Hyytiälä, Finland. We also quantify the PM mass of super-PM_{10} particles (Dp > 10 µm) via gravimetric analysis of cascade impactor filters to contextualize their sources, variability and impacts.~~Addressing these gaps requires a detailed investigation that accounts for both long-term trends and episodic variability. Our study offers a comprehensive analysis, focusing on the optical properties and PM mass of $PM_{1\text{-}10}$ aerosol particles, from the SMEAR II station in Hyytiälä, Finland, to improve the understanding of the sources, behavior, and impacts of $PM_{1\text{-}10}$ aerosol particles, which is essential for advancing knowledge of their role in atmospheric and climatic processes. While this study focuses on $PM_{1\text{-}10}$ particles, it also examines the PM mass of super-PM_{10} particles using gravimetric analysis of cascade impactor filters.~~ Specifically, this study aims to:

(a) Investigate the measurements of optical properties and mass of $PM_{1\text{-}10}$ aerosol particles at the SMEAR II station to analyze long-term trends of coarse-mode aerosol particles and their variability in boreal environments.

(b) Quantify the PM mass fraction of coarse-mode aerosol particles beyond the detection limits of optical instruments, constrained by the 10 µm size cut-off (super-PM_{10}), with implications for optical closure and vertical column density estimates.

(c) Assess the statistical significance of episodic events, such as pollen outbreaks and dust transport, on the optical properties of $PM_{1\text{-}10}$ aerosol particles.

(d) Examine the PM mass of the super-PM_{10} aerosol particles to fully capture the contributions of larger particles and their episodical significance in events such as pollen outbreaks or dust transport.

2. Measurement and methods

2.1 SMEAR II

The Station for Measuring Ecosystem–Atmosphere Relations (SMEAR II) is located in Hyytiälä, southern Finland (61°51'N, 24°17'E; 181 m.a.s.l.). It is located in a boreal forest and is classified as a background site where no major local sources of aerosol particles from anthropogenic activities are observed (Hari & Kulmala, 2005). However, there are some sources of pollution in the region, such as the city of Tampere (60 km in the southwest direction with a population of 241,000 in 2021) and the activity of the buildings in the station (Boy, 2004; Kulmala et al., 2001). Therefore, SMEAR II reflects typical boreal forest conditions~~Thus, SMEAR II represents the typical conditions that may be found in a boreal forest~~ (Hari et al., 2013). It has instruments to measure interactions between the forest ecosystem and the atmosphere~~. It is a part of the European Aerosols, Clouds, and Trace Gases Research Infrastructure or~~ and the station is part of ACTRIS (Laj et al., 2024). The station has various aerosol

instruments, including the four~~three~~ instruments used in this study: two~~a~~ Magee Scientific a~~a~~ethalometer~~s~~ (models AE31 and AE33) to obtain the light absorption coefficient at seven wavelengths, a TSI integrating nephelometer (model 3563) to calculate the light scattering coefficient at three wavelengths and a Dekati cascade gravimetric impactor to measure the PM mass of different size fractions (i.e. ≤ PM_1, between ~~≤~~ PM_1 and ~~-~~$PM_{2.5}$, between ~~-≤~~ $PM_{2.5}$ and ~~-~~PM_{10}, ≤ PM_{10}, > PM_{10}). The instruments are described in more detail in the following sections. All these instruments are in a *'Hitumökki,'* i.e., the 'Aerosol Cottage.'~~.~~

2.2 Measurement setup and instruments

The measurement setup for the aerosol optical instruments included a pre-impactor designed to remove the aerosol particles with a~~n~~ D_p >10 µm sampling PM_{10} aerosol particles. The inlet is located at a height of 8 m above ground inside the forest canopy. Following the pre-impactor, the airflow sequentially passed through an inlet flow splitter. This configuration allowed us to sample aerosol particles with aerodynamic diameter <1 µm (hereafter PM_1 aerosol particles) or PM_{10} every ten minutes. The switching inlet system has been described in detail by Luoma et al. (2021). Subsequently the size selected sample with a flow rate of 30 l min^{-1} is split into three streams to optical instruments.

One of the airstreams from the splitter goes into a Nafion dryer connected to an integrating nephelometer (TSI model 3563). With the Nafion dryer, the relative humidity of the sampled air is aimed to be kept ~~<~~below ~~4~~0%. The integrating nephelometer maintains a flow rate of 8.3 l ~~-~~min^{-1}.

The second airstream from the splitter passes through a different Nafion dryer and then enters the Magee Scientific aethalometer ~~(models AE31 and AE33)~~. The AE31 operated at SMEAR II until December 2017 and was replaced by the newer model AE33 in February 2018. The aethalometers maintain a flow rate of 5 l ~~-~~min^{-1}.

The third airstream is directed into a Thermo Fischer multi-angle absorption photometer (MAAP; model 5012) through a Nafion dryer. The MAAP maintains the flow rate of 16.7 l ~~-~~min^{-1}.

2.2.1 Aethalometer

The aethalometer quantifies the aerosol absorption coefficient (σ_{abs}) by measuring the reduction in light intensity as particles collect on a filter, facilitating continuous aerosol sampling (Zotter et al., 2017). The AE31 and AE33 models compare photon counts from light transmitted through a particle-laden filter spot to a clean reference filter. Correction algorithms account for aerosol particle scattering and multiple scattering within the quartz fiber filter. As light-absorbing particles build up, the effective optical path length shortens, necessitating adjustments for the filter-loading effect (Collaud Coen et al., 2010; Weingartner et al., 2003). The multiple-scattering correction factor (C_{ref}) addresses the enhancement of light scattering within the filter matrix due to the filter material, while the filter loading correction factor ($R(ATN)$) accounts for the non-linear instrument response caused by particle accumulation on the filter (Liousse et al., 1993). Since then, several studies have refined these correction approaches (Weingartner et al., 2003; Virkkula et al., 2007; Collaud Coen et al., 2010; Drinovec et al., 2015; Yus-Díez et al., 2021; Luoma et al., 2021).~~The multiple-scattering correction factor (C_{ref}) addresses the enhancement of light scattering within the filter matrix due to the filter material, while the filter loading correction factor ($R(ATN)$) accounts for the non-linear instrument response caused by particle accumulation on the filter (Liousse~~

et al., 1993). Further refinement in measurement accuracy is achieved by using single-scattering albedo (ω_0), which combines scattering and absorption coefficients to enhance the characterization of aerosol properties (Weingartner et al., 2003).

The Magee Scientific AE31 Aethalometer was operated at SMEAR II from October 2010 to December 2017 for continuous measurements of σ_{abs} at seven discrete wavelengths between 370 and 950 nm. Due to the single-spot filter design of the AE31, post-processing corrections were applied to account for artifacts arising from both multiple scattering within the quartz fiber filter matrix and the filter-loading effect. In this study, a C_{ref} of 1.57 was uniformly applied across all wavelengths, following the methodology presented by (Luoma et al., 2021). This value was derived using the correction algorithm developed by (Arnott et al., 2005), based on comparisons with absorption measurements from a Multi-Angle Absorption Photometer (MAAP) at the same site. The *R(ATN)* was also applied to compensate for the reduction in the effective optical path length as particles accumulated on the filter. These corrections were essential for ensuring accurate σ_{abs} retrievals and for addressing known biases in AE31 measurements associated with the scattering properties of the filter substrate. The corrected data enable reliable characterization of aerosol light absorption and its spectral dependence in the boreal environment.

From January 2018 to October 2022, the AE33 replaced the AE31 at SMEAR II. The AE33's dual-spot design corrects filter loading online (Drinovec et al., 2015), eliminating post-processing steps such as *R(ATN)*. In the AE33, the C_{ref} is a fixed, user-defined setting determined *apriori*—primarily by the filter tape—and remains constant during operation (AE33 User Manual, V1.56, August 2018). For consistency, we used two fixed values: C_{ref} = 1.57 for 2010–17 (AE31; Luoma et al., 2019) and C_{ref} = 1.39 for 2018–22 (AE33 with Magee M8060). Yus-Díez et al. (2021) showed that C_{ref} depends on both tape and aerosol optical properties; because their dataset did not include a low-altitude boreal background site comparable to SMEAR II, we did not apply additional site-specific or *SSA*-based adjustments. From January 2018 to October 2022, the AE33 aethalometer replaced the AE31 at the SMEAR II station. The AE33 incorporates a dual-spot filter design that continuously compares two filter spots with different particle loads, enabling real-time corrections for the filter-loading effect (Drinovec et al., 2015). Unlike the AE31, the AE33 does not require post-processing correction factors such as *R(ATN)*, as its dual-spot approach automatically compensates for loading effects during measurements. Additionally, the AE33 utilizes updated algorithms for scattering corrections, including adjustments to C_{ref}, improving measurement accuracy under varying aerosol concentrations and environmental conditions.

The key difference between the two instruments lies in their handling of the filter-loading effect. The AE31 requires manual post-processing to address non-linear responses caused by particle accumulation, while the AE33 performs these corrections in real time, reducing the need for post-processing and enhancing data reliability. This distinction, combined with the AE33's improved algorithms, allows for more accurate and consistent measurements of aerosol properties in dynamic environments.

2.2.2 Multi-angle absorption photometer

The Thermo Scientific model 5012 multi-angle absorption photometer (MAAP) measures light absorption coefficient and equivalent black carbon concentration at a 637 nm wavelength ($\sigma_{abs,637}$ and *eBC*, respectively) with a one-minute resolution and maintains a 16.67 lmin^{-1} airflow using an external pump. It collects aerosol particles

on glass fiber filter tape (Saturno et al., 2017). When particle accumulation reaches a threshold, the tape advances to a new place to avoid saturation. A 637 nm light source measures transmitted photon counts at a 0° detection angle, while reflected counts are measured at 130° and 165° to assess hemispheric backscattering (Petzold et al., 2005; Petzold & Schönlinner, 2004). The aerosol layer and filter matrix are modeled as a two-layer system, using the adding method and radiation budget equations (Petzold et al., 2005; van de Hulst, 1980). These equations are solved iteratively using the *SSA*~~single-scattering albedo~~ of the aerosol-loaded filter layer and layer optical depth until consistent values are reached (Petzold & Schönlinner, 2004). The *SSA*~~single-scattering albedo~~ is then used to calculate the aerosol mass and black carbon mass per unit volume, leading to the determination of $\sigma_{abs,637}$.

2.2.3 Integrating nephelometer

The TSI Incorporated model 3563 integrating nephelometer measures the light scattering and backscattering coefficients (σ_{sca} and σ_{bsca}, respectively) of the aerosol particles in their airborne state (Anderson et al., 1996). The instrument comprises three primary elements: a measurement chamber, a light source, and a detector. A diffuser guarantees that the light source emits a wavefront resembling a Lambertian distribution into the chamber. The chamber has a detector at one end and a light trap at the other. The chamber's interior is covered with black flocked paper to absorb stray light. The reference chopper positioned in front of the detector consists of three distinct sections: a signal section responsible for integrating light scattering within the range of 7° to 170°, a dark portion used to measure background noise, and a calibration section utilized to ensure the stability of the light source. A correction to address the scattering in blind angles (< 7° and > 170°) is applied according to Anderson and Ogren (1998).

A revolving backscatter shutter obstructs light within a scattering angle range of 7-90°, allowing for the measurement of hemispheric backscattering between 90° and 170°. The detector consists of three photomultiplier tubes and a lens that aligns dispersed light into parallel rays, dividing it into wavelengths of 450, 550, and 700 nm using dichroic and bandpass filters. The σ_{sca} and σ_{bsca} are determined by integrating the simplified scattering phase function. The data are corrected for gas molecule scattering by employing a HEPA filter. Regular span checks using CO_2 gas are conducted to account for instrument drift (Anderson et al., 1996).

2.2.4 Cascade impactor with subsequent gravimetric analysis

The sampling of ambient aerosol particles at SMEAR II has been conducted since the late 1990s using a Dekati PM_{10} cascade impactor filter with an unheated inlet for total suspended particulates (Laakso et al., 2003; Petäjä et al., 2025). The inlet, vertically sampling from approximately 5 m above ground level, consists of a stainless-steel tube with a rain cover. The impactor separates particles into three size fractions with aerodynamic diameter cut points at 10 µm (PM_{10}), 2.5 µm ($PM_{2.5}$), and 1 µm (PM_1) across its three stages. This separation is achieved with a consistent volumetric air flow rate of 30 l min^{-1} (Berner & Luerzer, 1980).

Collection substrates for the first two stages include 25 mm polycarbonate membranes (Nuclepore 800 203) without perforations. In contrast, the final stage employs a 47 mm Teflon filter with a 2 µm pore size (R2P J047) from Pall Corporation. To minimize particle rebound from the collection surfaces, the membranes are coated with a thin layer of Apiezon L vacuum grease and diluted in toluene. After collection, particulate samples are weighed in gravimetric analysis.

Particulate samples are weighed to produce aerosol mass distribution in two-to-three-day averages. The mass distributions are calculated based on the differences in filter weights before and after sampling. Once weighed, the filters are stored in a freezer to preserve the samples for future chemical and physical analyses. This procedure ensures the reliable collection, quantification, and archiving of aerosol particle data for long-term studies. The PM mass data across different aerosol particle size ranges, i.e. PM_1, PM_{10}, and super-PM_{10} (~~>PM_{10}~~) was merged with the hourly resampled aerosol optical properties (AOPs)~~y data~~.

2.3 Data processing of aerosol optical and PM mass-related properties

The aerosol optical data analyzed in this study span 4 October 2010 to 4 October 2022. Optical properties for the $PM_{1–10}$ size fraction were obtained by subtracting PM_1 measurements from the corresponding PM10 measurements of scattering and absorption. All optical time series were first resampled to hourly averages with a +30-minute offset, yielding timestamps centered at HH:30 (e.g., 00:30:00, 01:30:00, 02:30:00). This offset follows the EBAS convention maintained by NILU, in which hourly values are centered within their averaging intervals. The native temporal resolution of each instrument is listed in Table 1 and is preserved in the metadata; hourly resampling is used solely to align instruments with differing sampling cadences prior to subsequent aggregation.

To enable comparison with the impactor *PM mass* measurements, the optical data were averaged over the full duration of each impactor filter sampling interval, defined by the start–end timestamps of the sampling. For every interval, all optical points within the bounds were identified and averaged arithmetically, and the interval midpoint was used as the representative timestamp. The corresponding *PM mass* measurements were mapped onto the same intervals. Because filter samples typically span 2 to 3 days, these aggregated values are hereafter referred to as pseudo-daily mean values. This harmonization follows established practice for combining datasets with differing temporal resolutions and underpins the episodic and long-term analyses (Sheridan and Ogren, 1999; Collaud Coen et al., 2020); pollen events were classified from the 2–3-day filter samples, whereas dust events followed the day-specific scheme of Varga et al. (2023).

Additional processing ensured consistency across size cuts and instruments. All *PM mass* related-variables (*PM mass*, MSC_{550}: *mass scattering coeffcient at 550 nm* and MAC_{520}: mass absorption coefficient at 520 nm) were normalized by co-located dry *PM mass*, i.e. relative humidity (RH) ≤ 40%, for the same size fraction (PM_{10}, PM_1 and $PM_{1–10}$), with PM1–10 formed at the hourly step as PM_{10} and PM_1, prior to aggregation to the impactor filter intervals. Scattering coefficients were measured at low RH and corrected for angular truncation and non-ideal angular response (Anderson and Ogren, 1998; Müller et al., 2011). Light absorption coefficient at 520 nm ($\sigma_{abs,520}$) was obtained from AE31 (2010–2017) and AE33 (2018–2022), with the AE33 dual-spot loading correction applied as provided (Drinovec et al., 2015). These harmonized and corrected optical timeseries, aligned to the filter sampling windows, provide a consistent basis for the subsequent seasonal and trend evaluations of both optical and mass-based aerosol properties (Sheridan and Ogren, 1999; Collaud Coen et al., 2020; Varga et al., 2023; Anderson and Ogren, 1998; Müller et al., 2011; Drinovec et al., 2015).~~The aerosol optical data analyzed in this study cover the period from 4 October 2010 to 4 October 2022. Optical properties for the $PM_{1–10}$ aerosol particle size fraction were derived by subtracting PM_1 aerosol particle measurements from the corresponding PM_{10}~~

~~aerosol particle measurements of scattering and absorption. All optical data were initially resampled to hourly averages using a +30-minute offset, resulting in timestamps centered at, for example, 00:30:00, 01:30:00, 00:02:30 and so on. This offset reflects the standard timestamp convention used by the Environmental Database for Atmospheric Studies (EBAS), maintained by the Norwegian Institute for Air Research (NILU), where hourly values are centered within their respective averaging intervals. The actual temporal resolution of each instrument is listed in Table 1.~~

~~To enable comparison with the gravimetric PM mass measurements, the optical data were subsequently averaged within each filter sampling interval, as defined by the start and end timestamps of the impactor measurements. This was achieved by identifying overlapping timestamps between the optical and gravimetric datasets and computing the mean of the optical variables within each sampling window. The corresponding PM mass and metadata from the filter dataset were assigned to the same time windows in the optical dataset. This procedure yielded a set of time-aligned values, hereafter referred to as '*pseudo-daily mean values*'. These values provided the basis for subsequent seasonal and long-term analyses across optical and mass-based variables.~~

~~Hourly optical data were converted to pseudo-daily means primarily because pollen events were classified based on filter samples collected every two to three days. In contrast, the specific days on which dust events occurred were identified using the event classification presented by (Varga et al., 2023). The use of pseudo-daily resolution ensures consistency between the time bases of the optical and mass measurements, particularly for the episodic analysis. For this reason, all optical data were first resampled to the hourly timescale to facilitate precise temporal alignment and averaging across the datasets before aggregation into analysis-ready values.~~

Table 1. Temporal resolutions and size cut-offs of the different aerosol optical instruments

Instrument	**Temporal resolution**	**Size cut-off**
Aethalometer (AE33)	2 minutes	PM_1, PM_{10}
Multi angle absorption photometer (MAAP; Thermo Scientific model 5012)	1 minute	PM_1, PM_{10}
Integrating nephelometer (TSI Incorporated model 3563)	1 minute	PM_1, PM_{10}
Dekati Gravimetric Cascade Impactor (GCI)	2-3 days	$\leq PM_1$, $\leq PM_1$-$PM_{2.5}$, $\leq PM_{2.5}$-PM_{10}, $\leq PM_{10}$, $> PM_{10}$

In this study, we analyzed absorption data for both PM_1 and PM_{10} aerosol particles. Specifically, we utilized the MAAP data to plot $\sigma_{abs,637}$, and the AE31/33 data to plot $\sigma_{abs,660}$. Subsequently, a scatterplot was created with the MAAP data to plot $\sigma_{abs,637}$ on the x-axis and the AE31/33 data to plot $\sigma_{abs,660}$ on the y-axis. This allowed us to determine the slope and y-intercept, which were then used to scale $\sigma_{abs,660}$ data from the AE31/33 instruments to

match $\sigma_{abs,637}$ from the MAAP instrument~~s~~. The same correction factors (slope = 2.33~~6~~ and y-intercept = -0.16~~8~~; Figure S9) derived from this analysis were extended to scale the σ_{abs} data from the AE31/33 instrument at the other six wavelengths of 370, 470, 520, 550, 880 and 950 nm to correct all the data from the AE31/33 instruments.

For calculating the trends in the different aerosol optical data, the Mann-Kendall regression was used to effectively handle outliers without assuming a normal distribution (Collaud Coen et al., 2020). This method also minimizes the risk of Type I errors, which can occur when a trend is incorrectly identified as *'statistically significant'* due to an anomaly in the data (i.e., autocorrelation). Additionally, Sen-Theil's slope estimator has been used to quantify the slope of the trends, providing a reliable measure of the long-term changes in the aerosol optical properties, even if there are non-linear trends and seasonal fluctuations in the data (Collaud Coen et al., 2020).

Equation (1) was used to calculate the relative slope:

$$\text{Relative slope } (\%\text{yr}^{-1}) = \left(\frac{\text{Sen-Theil's slope}}{\text{Median of aerosol optical data}} \times 365.25\text{yr}^{-1} \times 100\%\right), \quad (1)$$

Two key parameters used to characterize the wavelength dependence of the ~~aerosol optical properties (~~AOPs~~)~~ are the Absorption Ångström Exponent (*AAE*) and the Scattering Ångström Exponent (*SAE*). These exponents provide insights into aerosol composition and particle size distributions, offering indirect information about the types of aerosols present. While they are not directly used to estimate climate effects, they are important for understanding the physical and chemical properties of aerosols, which influence their behavior and interactions with radiation. ~~Two key parameters that are routinely used to characterize the wavelength dependence of AOPs are the Ångström exponents: the *AAE* and the *SAE*.~~

2.3.1 Absorption Ångström exponent (*AAE*)

The *AAE* represents the wavelength dependence of aerosol light absorption and provides insights into the chemical characteristics of aerosol particles, such as brown carbon (BrC) or presence of coatings on a BC core, which have important implications for radiative forcing (Cazorla et al., 2013). The AAE was calculated by determining the slope of the ordinary least squares (OLS) linear fit of the natural logarithmic values of the σ_{abs} as a function of wavelength:

$$AAE = -\frac{\Delta \ln(\sigma_{abs,\lambda})}{\Delta \ln(\lambda)}, \quad (2)$$

where σ_{abs} represents the light absorption coefficient at wavelength λ. For AAE, absorption measurements are taken at the following 7 wavelengths: 370, 470, 520, 590, 660, 880~~,~~ and 950 nm.

2.3.2 Scattering Ångström exponent (*SAE*)

The *SAE* quantifies the wavelength dependence of aerosol light scattering and is closely associated with aerosol particle size distribution. Higher *SAE* values generally indicate a dominance of smaller, fine-mode particles, which exhibit a stronger wavelength dependence in scattering behavior. Conversely, lower *SAE* values are associated with larger, coarse-mode particles that scatter light more uniformly across wavelengths. This relationship makes the *SAE* a valuable metric for assessing aerosol size distributions, providing insight into the relative abundance of

fine and coarse particles and their implications for atmospheric radiative properties and climate-forcing (Schuster et al., 2006).

In this study, the *SAE* was calculated similarly to the *AAE* by applying an Ordinary Least Squares (OLS) linear regression to the natural logarithmic values of the light scattering coefficients at 450, 550, and 700 nm, regressed against the natural logarithmic values of these wavelengths, as shown in Equation 3:

$$SAE = -\frac{\Delta \ln(\sigma_{sca,\lambda})}{\Delta \ln(\lambda)}, \quad (3)$$

2.3.3 Single scattering albedo (*SSA*)

The *SSA* is a key aerosol optical property that is defined as the ratio of the σ_{sca} to the total extinction coefficient (the sum of σ_{sca} and σ_{abs}). The *SSA* is instrumental in determining whether aerosols exert a net cooling or warming effect on the atmosphere: higher *SSA* values generally indicate that aerosols are primarily scattering, contributing to a cooling effect, while lower *SSA* values suggest a more significant role in absorption, which leads to warming (Bond et al., 2013; Luoma et al., 2019; Tian et al., 2023). *SSA* can be calculated at any wavelength; in this study, *SSA* was calculated explicitly at 550 nm (hereon SSA_{550}).

2.3.4 Mass absorption coefficient (*MAC*)

The *MAC* represents the efficiency with which aerosol particles absorb light per unit mass (not to be confused with *MAC* of BC, which is used in conversion of σ_{abs} to BC mass). The *MAC* is sensitive to changes in aerosol chemical composition and is a valuable indicator of shifts in absorbing components, such as BC and certain light absorbing organic compounds (i.e., BrC). These changes in the *MAC* often reflect variations in aerosol sources or chemical aging processes (Andreae & Gelencsér, 2006; Bond & Bergstrom, 2006). Long-term studies on *MAC* can reveal trends in aerosol composition, especially in regions like the Arctic and boreal environments, where variations in pollution sources and climate-driven changes are prevalent.

2.3.5 Mass scattering coefficient (*MSC*)

The *MSC* quantifies the efficiency with which aerosol particles scatter light per unit mass. In contrast to the *MAC*, the *MSC* is primarily influenced by the physicochemical~~al~~ characteristics of aerosols—especially particle size, shape, and composition—as these properties impact light-scattering efficiency per unit mass (Bates et al., 2005; Seinfeld & Pandis, 2016). Higher *MSC* values are typically associated with a more significant proportion of scattering particles, such as sulfate, nitrate, and other non-absorbing components, which contribute to a cooling effect in the planetary boundary layer (PBL), partially counteracting the warming effect of absorbing aerosols (Pandolfi et al., 2014).

3. Results and discussion

3.1 General characteristics of PM_{1-10} aerosol particles

Long-term observations at SMEAR II indicate that $PM_{1–10}$ primarily contributes to aerosol scattering, with minimal absorption due to its composition, which is predominantly influenced by aerosol particles of biogenic origin (e.g., pollen, fungal spores) and mineral dust (Luoma et al., 2019; Zieger et al., 2015). The *SSA* remains consistently high (>0.90), while the *MSC* is lower than that of PM_1, aligning with Mie theory predictions for larger particles (Pandolfi et al., 2018; Titos et al., 2021). A summary of these descriptive statistics for PM1–10 aerosol particles is provided in Table 2. Seasonal variations reveal increased $PM_{1–10}$ scattering during spring and early summer due to enhanced biogenic activity, particularly from pollen and fungal spores (Heikkinen et al., 2020; Yli-Panula et al., 2009), whereas winter conditions favor fine-mode aerosols, reducing the relative contribution of $PM_{1–10}$ (Luoma et al., 2021).

Intermittent mineral dust intrusions, predominantly from the Aral-Caspian region, contribute to episodic increases in atmospheric dust concentrations over Finland (Varga et al., 2023). While these events introduce coarse-mode aerosols, their influence on the absorption properties of $PM_{1–10}$, particularly in terms of MAC variability, remains poorly characterized due to limited long-term observations and uncertainties in aerosol source contributions. Lihavainen et al. (2015) analyzed long-term aerosol optical properties at the Pallas Global Atmospheric Watch station, focusing on PM_{10} rather than specifically $PM_{1–10}$, but their findings on seasonal variations in scattering and absorption provide useful context for interpreting boreal aerosol trends.

Hygroscopic growth measurements suggest that $PM_{1–10}$ is less effective as cloud condensation nuclei (CCN) compared to fine-mode aerosols, influencing its atmospheric lifetime and radiative effects (McFiggans et al., 2006). While Lihavainen et al. (2015) examined aerosol hygroscopic properties in northern Finland, their study primarily covered PM_{10} rather than isolating the $PM_{1–10}$ fraction. The contribution of $PM_{1–10}$ to total PM_{10} scattering at SMEAR II remains substantial, though its representation in optical measurements is uncertain due to limitations in nephelometry and aethalometry, which tend to underestimate coarse-mode aerosol properties (Brasseur et al., 2024; Zieger et al., 2015).

Table 2. Descriptive statistics of the aerosol optical properties for all the valid data of the PM_{1-10} particles.

		Wavelength (nm)	**$PM_{1–10}$ aerosol particles**				
Extensive variables			25%ile	Mean	Median	75%ile	Std. dev.
	σ_{abs} *(Mm^{-1})*	520	0.070.09	0.170.18	0.120.14	0.210.22	0.180.16
	σ_{sca} *(Mm^{-1})*	550	1.491.75	3.153.35	2.392.75	3.924.19	2.782.55
	PM mass (μgm^{-3})		0.900.970	2.202.33	1.511.580	2.452.55	3.223.51
Intensive variables	*AAE (dimensionless)*	370-950	0.540.57	0.730.73	0.730.74	0.910.89	0.450.33
	SAE (dimensionless)	450-700	0.130.11	0.380.24	0.360.32	0.690.58	0.600.81
	SSA (dimensionless)	550	0.930.93	0.930.94	0.950.95	0.960.96	0.370.04
	MAC (m^{2}g^{-1})	520	1.030.05	2.030.11	1.580.08	2.520.14	10.790.86

	MSC (m^2g^{-1})	550	0.041.07	0.121.92	0.081.61	0.132.65	0.9111.64

3.2 Long-term trends of extensive properties

Extensive properties refer to the properties of aerosol particles that depend on the amount of the aerosol particles. From the studied extensive properties, $\sigma_{sca,550}$, $\sigma_{abs,520}$ and mass for PM_{1-10} aerosol particles show a clear long-term negative trend from October 2010 to October 2022, reflecting a decline in optical and mass properties (Figure. 1). To compare the relative differences with PM_{1-10}, trends for PM_1 and PM_{10} size fractions are also studied, and all the trends are presented in Table 3.

This decrease aligns with earlier findings at SMEAR II, as reported by Luoma et al. (2019), where reductions in extensive properties were attributed to declines in particle number concentration and volume concentrations, particularly impacting larger accumulation mode and coarse-mode aerosol particles with peaks at approximately 700 nm and 5 µm, respectively.

Pollen and dust events (green and red stars; Sect. 2.3) introduce additional short-term variability in the observed optical and mass properties without altering the sign or statistical significance of the long-term trends (Table 3). Pollen and dust events, marked as green and red stars in all figures where they are plotted, contribute additional variability to the observed optical and mass properties. Pollen events are typically seasonal, occurring during spring and summer, and contribute significantly to particle mass and scattering in the PM_{1-10} size range. Dust events, which are more intermittent and often result from long-range transport, enhance scattering and mass concentrations in the coarse mode, including PM_{1-10} aerosol particles. While these events introduce short-term variability, they do not alter the overall long-term declining trends. The pseudo-daily mean values used in this analysis help to better highlight such events by providing a finer temporal resolution, enabling the identification of short-term peaks in optical and mass properties alongside the broader trends.

Table 3. Long-term trends and statistical significance of PM_{1-10} aerosol optical and PM_{1-10} mass properties.

S. No.	Variable	Slope	Relative trend	p-value	Statistical significance
(a)	$\sigma_{sca,\,550}$ *(Mm^{-1})*	-0.051.05 x 10^{-2} ± 0.040.05 $Mm^{-1}yr^{-1}$	-1.930.39 ± 1.741.67 $\%yr^{-1}$	0.160.71	NoNo
(b)	$\sigma_{abs,\,520}$ *(Mm^{-1})*	-9.83-9.57 x $10^{-3}10^{-3}$ ± 2.282.46 x $10^{-3}10^{-3}$ $Mm^{-1}yr^{-1}$	-8.02-7.38 ± 1.861.90 $\%yr^{-1}$	0.0526.23 x 10^{-11}	NoYes
(c)	*SAE (dimensionless)*	-0.03-0.05 ± 0.020.02 yr^{-1}	-7.30-12.83 ± 4.164.63 $\%yr^{-1}$	3.010.08 x 10^{-8}	NoYes
(d)	*AAE (dimensionless)*	0.030.03 ± 8.637.86 x $10^{-3}10^{-3}$ yr^{-1}	3.544.60 ± 1.041.09 $\%yr^{-1}$	1.786.73 x $10^{-3}10^{-13}$	Yes
(e)	*PM mass (μgm^{-3})*	-0.04-0.04 ± 0.010.04 $\mu gm^{-3}yr^{-1}$	-2.61-2.94 ± 1.002.43 $\%yr^{-1}$	0.060.02	NoYes

S. No.	Variable	Slope	Relative trend	p-value	Statistical significance
(f)	SSA_{550} *(dimensionless)*	1.942.63 x 10^{-3}10^{-3} ± 7.758.88 x 10^{-4}10^{-4} yr^{-1}	0.200.28 ± 0.080.09 %yr^{-1}	0.101.31 x 10^{-7}	NoYes
(g)	MSC_{550} *(m^2g^{-1})*	-0.02 6.43x 10^{-3}-± 1.07 x 10^{-2}0.01 $m^2g^{-1}yr^{-1}$	-1.130.39 ± 0.94-0.66 %yr^{-1}	0.500.22	No
(h)	MAC_{520} *(m^2g^{-1})*	-2.77-2.66 x 10^{-3}10^{-3} ± 9.046.69 x 10^{-4}10^{-4} $m^2g^{-1}yr^{-1}$	-3.97-3.47 ± 1.300.87 %yr^{-1}	0.021.44 x 10^{-14}	Yes

719

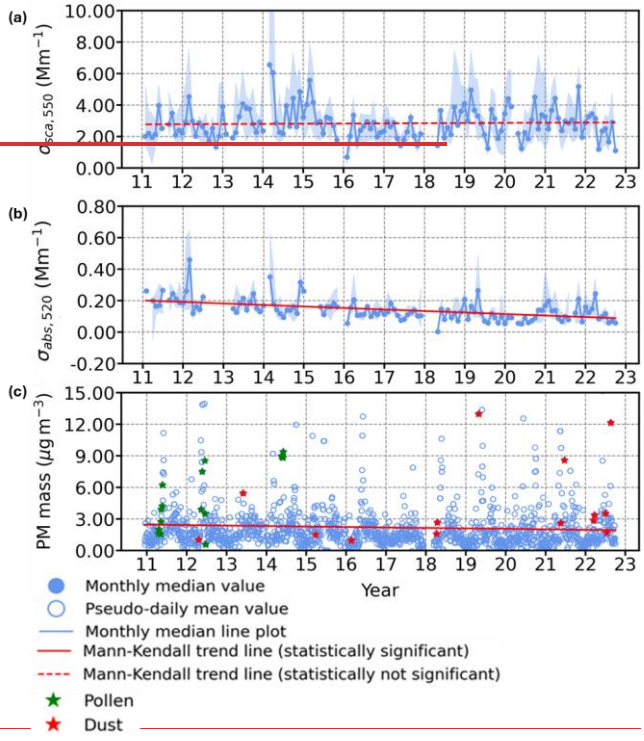

720

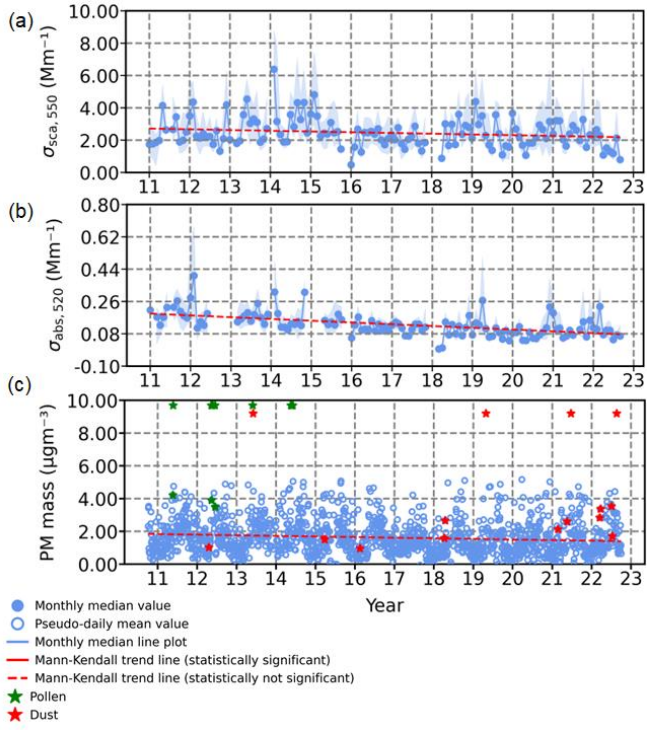

Figure 1. Time series of (a) $\sigma_{sca,550}$, (b) $\sigma_{abs,520}$ and (c) *PM mass* for the $PM_{1–10}$ size aerosol particles from October 2010 to October 2022. The blue shaded area is the interquartile range (25th–75th percentile) of monthly values; the blue line is the monthly median. The red line shows the Theil-Sen trend (solid if $p \leq 0.05$; dashed otherwise). Months with <75% data coverage are left blank.

3.2.1 Light ~~s~~Scattering coefficient at 550 nm ($\sigma_{sca,550}$)

Scattering due to PM_1 aerosol particles at SMEAR II shows a long-term decrease (slope: -0.29 ± 0.15 $Mm^{-1}yr^{-1}$; relative trend: -4.80 ± 2.43 $\%yr^{-1}$; Figure S2(a); Table S4(a)). ~~Scattering due to PM1 aerosol particles at SMEAR II shows a trend of −0.26 ± 0.17 Mm^{-1} yr^{-1}; −3.48 ± 2.33 % yr^{-1} (Figure S2(a); Table S4(a)).~~ Submicron particles dominate aerosol light scattering at the site (Virkkula et al., 2011), suggesting that $\sigma_{sca,550}$ is influenced primarily by fine-mode aerosol loading. The observed negative trend is consistent with reductions in anthropogenic sulfur dioxide (SO_2) emissions, which contribute to secondary sulfate formation, a major component of PM_{1+} aerosol mass and associated optical properties (Smith et al., 2011). Regionally, similar decreases in aerosol scattering have been reported at multiple European background stations (Pandolfi et al., 2018), further supporting the possibility of a widespread decline in fine-mode aerosol scattering. SMEAR II is also subject to seasonal biogenic emissions, particularly monoterpenes that contribute to secondary organic aerosol (SOA) formation (Hakola et al., 2003; Hallquist et al., 2009; Rantala et al., 2015). However, long-term records indicate that B ~~biogenic~~ VOC emissions at this site have remained relatively stable over the past two decades (Kulmala et al., 2001). As such,

no evidence currently supports a significant contribution of BVOC variability to the observed multi-year decline in PM_{1} ~~1~~ scattering. Taken together, the trend observed at SMEAR II is consistent with known reductions in anthropogenic precursor emissions, particularly SO_{2}~~2~~, though additional factors cannot be excluded.

3.2.2 Light a~~A~~bsorption coefficient at 520 nm ($\sigma_{abs,\,520}$)

For PM_{10} and PM_{1}, $\sigma_{abs,520}$ decreases significantly over the record. PM_{10} declines at -0.11 ± 0.03 Mm^{-1} yr^{-1} (-8.75 ± 2.11 % yr^{-1}; Fig. S1b; Table S3b), and PM_{1} at -0.09 ± 0.02 Mm^{-1} yr^{-1} (-8.87 ± 2.18 % yr^{-1}; Fig. S2b; Table S4b). Both series exhibit winter maxima and a recurring late-spring minimum, in agreement with the established seasonal cycle at SMEAR II (Luoma et al., 2019) and consistent with Europe-wide declines in aerosol absorption and black-carbon emissions (Collaud Coen et al., 2020; Yttri et al., 2021).

The close agreement of the relative declines indicates that the PM_{10} absorption trend is likely dominated by the fine-mode (PM_{1}) contribution at 520 nm, based on the corrected and harmonized time series described in Section 2.3. For physical context—not used in estimating the trends reported above—coarse-mode particles typically contain weakly absorbing mineral and biological components (Laskin et al., 2005; Moosmüller et al., 2009) and have shorter atmospheric residence times due to gravitational settling (Emerson et al., 2020; Zhang et al., 2001). Considerations related to long-term sensitivity, harmonization, and instrument intercomparison are documented elsewhere (Collaud Coen et al., 2010) and do not affect the magnitude or direction of the PM_{10}/PM_{1} trends summarized here.

3.2.3 PM mass concentration (*PM mass*)

Although this study focuses on PM_{1} and $PM_{1\text{-}10}$ fractions, investigating trends in super-PM_{10} aerosol particles~~s~~ may provide additional insights into long-term shifts in coarse-mode aerosol composition that are not detected by the optical instruments and the used 10 µm cut-off. Super-PM_{10} particles, which include biological aerosols (e.g., pollen, fungal spores) and mineral dust, are strongly influenced by episodic events such as seasonally driven biological emissions and long-range dust transport. However, their long-term trends remain poorly constrained.

The variability in super-PM_{10} aerosols likely reflects a combination of natural and anthropogenic influences. While mineral dust and pollen contribute significantly to coarse-mode particles, their variability is largely seasonal and event-driven. In contrast, fine-mode aerosol particles (PM_{1}) and $PM_{1\text{-}10}$ aerosol particles~~s~~ exhibit more consistent long-term trends due to anthropogenic emissions. The decline in PM_{1} mass concentrations aligns with reductions in both primary and secondary anthropogenic aerosol sources. However, $PM_{1\text{-}10}$ contains a larger fraction of natural aerosols, which exhibit substantial variability but may not necessarily follow a long-term trend.

Previous studies (Leskinen et al., 2012; Varga et al., 2023) have highlighted the episodic nature of coarse-mode aerosol contributions, including periods of increased dust transport to Finland, particularly after 2010 (Varga et al., 2023). The frequency of these events, combined with changes in regional meteorology and source contributions, may introduce variability in observed $PM_{1\text{-}10}$ trends. In this study, we further assess the relative contributions of biological aerosols and mineral dust by comparing super-PM_{10} variations with $PM_{1\text{-}10}$, providing insights into their role in long-term aerosol trends and atmospheric transport patterns.

3.3 Long-term trends of intensive properties

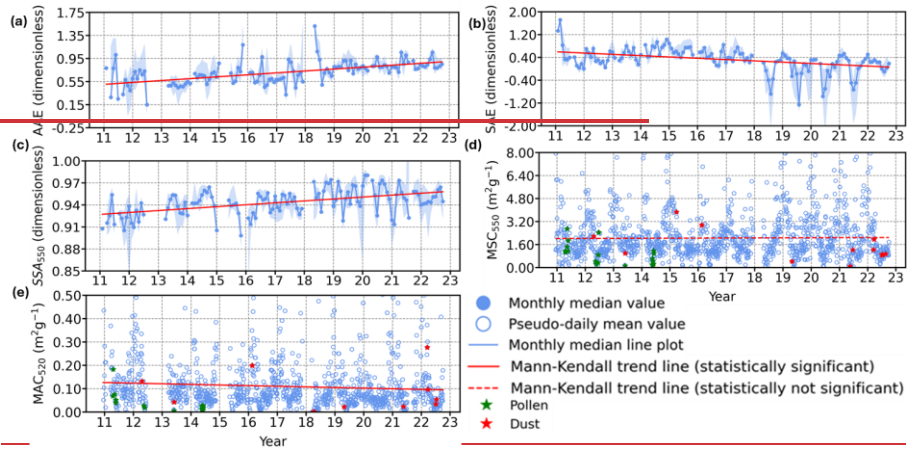

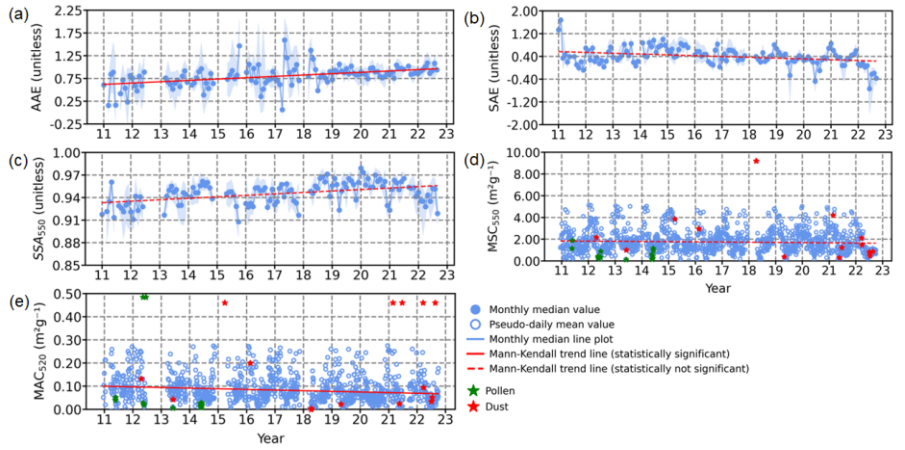

Figure 2. Time series of (a) *AAE*, (b) *SAE*, (c) SSA_{550}, (d) MSC_{550} and (e) MAC_{520} for the $PM_{1–10}$ aerosol particles from October 2010 to October 2022. The blue shaded area is the interquartile range (25th–75th percentile) of monthly values; the blue line is the monthly median. The red line shows the Theil-Sen trend (solid if $p \leq 0.05$; dashed otherwise). Months with <75% data coverage are left blank.

3.3.1 Absorption Ångström exponent (*AAE*)

The *AAE* for $PM_{1–10}$ aerosol particles exhibits a statistically significant decreasing trend with a slope of 0.03 ± ~~8.63 x 10^{-3} yr^{-1}~~ ~~0.03 ± 7.86 × 10^{-3} yr^{-1}~~; 3.54 ± 1.04 %yr^{-1} ~~4.60 ± 1.09 %yr^{-1}~~ (Figure 2(a); Table 3(d)), suggesting a shift in aerosol composition. ~~PM_{10} aerosol particles also display a negative trend of −1.13 × 10^{-2} ± 5.03 × 10^{-3} yr^{-1}; −1.01 ± 0.45 %yr^{-1} (Figure S3(a); Table S3(d)), while PM_1 aerosol particles exhibit a smaller but still decreasing~~

~~trend of -1.37 × 10^{-2} ± 6.29 × 10^{-3} yr^{-1}, -1.16 ± 0.54 %yr^{-1} (Figure S4(a); Table S4(d)), which could be attributed to the dominance of BC in the fine aerosol particle fraction.~~ The more pronounced decrease in $PM_{1–10}$ suggests a potential decline in BrC, possibly due to enhanced oxidation processes or a shift toward less absorbing organic aerosols. This aligns with long-term reductions in BC concentrations at Hyytiälä (Luoma et al., 2021) and shifts in organic aerosol sources (Äijälä et al., 2019; Heikkinen et al., 2020). Given that BC is predominantly submicron, the decreasing *AAE* in $PM_{1–10}$ is more likely to reflect changes in BrC absorption characteristics in the coarse-mode fraction rather than BC variability alone.

A notable abrupt change in *AAE* values is observed between pre-2018 and post-2018, which may be linked to the instrumental transition from AE31 to AE33 in March 2018. The AE33 a~~A~~ethalometer introduces real-time filter-loading corrections through a dual-spot measurement approach, which effectively reduces filter-loading biases inherent to the AE31 model (Drinovec et al., 2015). This methodological difference has been shown to impact BC and BrC estimates, particularly influencing *AAE* calculations (Backman et al., 2017; Zotter et al., 2017). Also, Luoma et al. (2021) showed how *AAE* varies between different aethalometer correction algorithms. Interestingly, this discontinuity is not observed in PM_1 or PM_{10} *AAE* trends, which suggests that the AE31-to-AE33 transition might have introduced size-dependent effects in *AAE* calculations. Previous studies indicate that AE33 generally yields lower *AAE* values than AE31, especially at shorter wavelengths where BrC absorption dominates, which could affect how BrC in coarse-mode aerosols ($PM_{1–10}$) is quantified (Bernardoni et al., 2021; Zotter et al., 2017).

While these differences align with known AE31-to-AE33 biases, further analysis is needed to determine whether the observed *AAE* shift stems solely from instrumental changes or also reflects atmospheric variations. Examining the *AAE* wavelength dependence across size fractions and assessing potential modifications in BrC optical properties could help separate instrumental artifacts from real aerosol composition trends. At least one previous study, Bali et al. (2024), highlights the importance of BrC optical properties in interpreting long-term aerosol trends, particularly in environments influenced by SOA and episodic biomass-burning events.

3.3.2 Scattering Ångström exponent (*SAE*)

The *SAE* for PM_{1-10} particles exhibits a negative trend of -0.03 ± 0.02 yr^{-1} ~~-0.05 ± 0.02 yr^{-1}~~; -7.30 ± 4.16 %yr^{-1} ~~-12.83 %yr^{-1}~~ (Figure 2(b); Table 3(c)), indicating a declining influence of smaller particles (closer to 1 µm) or a slower decline of larger particles (closer to 10 µm), given concurrent decreases in $\sigma_{sca,550}$ and *PM mass*. This suggests that fine-mode aerosols within PM_{1-10} are decreasing at a faster rate than those in the 2.5–10 µm range, leading to a relative dominance of larger particles rather than an absolute increase. The observed trend may be driven by reduced secondary aerosol formation or changes in atmospheric processing (Maso et al., 2005; Seinfeld & Pandis, 2016). A decline in fine-mode SOA condensation onto pre-existing particles could limit fine-mode growth, shifting the relative contribution of supermicron particles (>1 µm). Additionally, long-term reductions in sulfate emissions make it unlikely that an increase in sulfate mass is responsible for the shift in *SAE*. Instead, changes in dust concentrations could play a role, although long-term dust trends remain uncertain. The negative *SAE* trend observed for PM_{10} (Figure S3(~~,~~b)) further suggests a greater relative contribution of larger particles within PM_{10}, likely due to a slower decline in the 2.5–10 µm range compared to fine-mode particles (1–2.5 µm). Aerosol particles in this size range, including mineral dust, sea salt, pollen~~,~~ and fungal spores, exhibit different atmospheric lifetimes and removal processes than finer particles, contributing to differences in observed trends.

For PM_1 (Figure S4(b)), *SAE* remains stable, suggesting no major shifts in fine-mode size distributions. This stability indicates that the ratio of BC to scattering components, primarily sulfate and organics, has not changed significantly over time. Luoma et al. (2019) reported a decrease in volume mean diameter (VMD) from ~0.25 µm to ~0.2 µm (2006–2017), indicating a long-term shift toward smaller aerosol sizes. While this period does not fully overlap with this study, the trend likely continued, though more recent data would be needed to confirm this assumption. The observed differences between PM_1 and $PM_{1\text{-}10}$ *SAE* trends highlight the distinct processes influencing fine and larger aerosols, including atmospheric processing, long-range transport, and primary emissions. Reduced SOA condensation onto fine particles may further enhance the relative contribution of larger particles in PM_{10}. However, while pollen (>10 µm) is classified as a coarse aerosol in this study, its influence on *SAE* trends is likely minimal, as infrequent high concentrations from pollen events are statistically down-weighted in the calculation of monthly medians. The concurrent decline in $\sigma_{sca,550}$ and *PM mass* indicates that the negative *SAE* trend is not due to an absolute increase in large particles but rather a differential reduction in size fractions. Together, these findings suggest that ongoing changes in secondary aerosol formation and primary emissions are influencing the evolution of aerosol size distributions in different size fractions.

3.3.3 Single scattering albedo (SSA_{550})

The SSA_{550} for PM_{10}, PM_1, and PM_{1-10} shows no statistically significant long-term trends over the measurement period (Figures 1(c), 2(c), 3(c); Table 3(f)). Statistical significance was evaluated using the Mann–Kendall test (p compared with 0.05) and Theil–Sen slopes with 95 % confidence intervals. Although the fitted slopes are positive across all size fractions, they are not significant and cannot be interpreted as evidence of systematic long-term changes in the balance between scattering and absorbing components. The lack of statistically significant trends likely reflects the relatively short record (~2010–2022), the high natural variability of SSA_{550} driven by meteorology, regional and long-range transport, and episodic contributions from pollen and mineral dust. These influences are particularly strong in the coarse and supermicron fractions, where sporadic sources dominate, limiting the statistical power to resolve weak tendencies. The absence of concurrent long-term chemical composition and source-apportionment datasets further constrains attribution of SSA_{550} variability to specific aerosol species or emission changes.

Changes in *SSA* are generally associated with reductions in absorbing components, such as black carbon, or increases in non-absorbing species, such as sulfates and organics (Bond et al., 2013; Luoma et al., 2019; Pandolfi et al., 2014). However, regional SO_2 emissions have declined substantially over recent decades (Klimont et al., 2013), making a sulfate-driven increase in SSA_{550} at Hyytiälä unlikely. Long-term measurements at the site show that organic aerosol dominates the aerosol mass fraction, with variability largely seasonal rather than indicative of sustained long-term changes (Heikkinen et al., 2021; Äijälä et al., 2019). Without detailed separation of primary and secondary organic aerosol and the absence of continuous long-term dust measurements, it remains difficult to evaluate whether any weak tendencies toward increased scattering are linked to changes in mineral dust or other primary sources. Overall, the SSA_{550} observations indicate that the relative balance between scattering and absorbing aerosol components has remained broadly stable at Hyytiälä over the past decade.

Formatted: Font: Italic

Formatted: Font: Italic

Formatted: Font: Italic, Subscript

Formatted: Font: Italic

Formatted: Font: Italic, Subscript

~~The SSA_{550} for PM_{1-10} particles exhibits a small positive trend with a slope of $2.63 \times 10^{-3} \pm 8.88 \times 10^{-4}$ yr^{-1}; 0.28 ± 0.09 $\%yr^{-1}$ (Figure 2(c); Table 3(f)), indicating an increase in scattering relative to absorption. This trend has been attributed to reductions in BC contributions or increases in non-absorbing components such as sulfates and organic matter (Bond et al., 2013; Luoma et al., 2019; Pandolfi et al., 2014). However, these references provide general evidence on aerosol composition rather than site-specific confirmation for Hyytiälä. Given the decline in SO_2 emissions over recent decades, a significant increase in sulfate in the coarse fraction appears unlikely. Instead, an enhanced contribution from mineral dust, a known scattering agent, could provide a more plausible explanation. However, trends in dust concentrations at the site remain uncertain due to a lack of direct long-term observations. A similar increasing SSA_{550} trend is observed for PM_{10} particles (Figure S3(c)), reinforcing the hypothesis that larger particles within PM_{10} are playing a greater role in scattering. In contrast, SSA_{550} for PM_1 particles (Figure S4(c)) remains stable, suggesting no significant long-term shift in the relative proportions of absorbing and scattering aerosols in the fine mode. This stability does not necessarily indicate the dominance of strongly absorbing BC but rather suggests that the ratio of BC to scattering components, primarily sulfate and organics, has not changed significantly over time.~~

~~Long-term chemical composition measurements at Hyytiälä provide additional insight into these trends. Heikkinen et al. (2021) and Äijälä et al. (2019) reported that organic aerosol remains the dominant fraction, but its variations have been largely seasonal rather than indicative of a sustained long-term increase. OA consists of both primary organic aerosol (POA), which is directly emitted from sources such as biomass burning and fossil fuel combustion, and SOA, which forms through gas-phase oxidation of volatile organic compounds (VOCs). While these studies discuss OA in the context of its chemical composition and seasonal variations, they do not explicitly distinguish between POA and SOA when assessing long-term trends. Additionally, ammonium sulfate, a key scattering component, has not shown an increasing trend in the coarse fraction that would explain the observed SSA rise in PM_{1-10} and PM_{10}. The increase in SSA_{550} in these size fractions may instead be influenced by changes in dust concentrations or primary aerosol sources, though direct evidence for these trends at Hyytiälä is lacking. While mineral dust is a plausible explanation for the increase in SSA_{550}, long-term regional data on dust concentrations are needed to confirm this hypothesis. The observed stability of SSA_{550} in PM_1 particles further suggests that the balance between absorbing and scattering components in the fine mode has remained relatively unchanged. This indicates that while SSA_{550} trends in PM_{1-10} and PM_{10} may be influenced by shifts in scattering aerosol composition, the fine mode remains relatively stable in its overall composition.~~

3.3.4 Mass scattering coefficient (MSC_{550})

From October 2010 to October 2022, the PM_{1-10} MSC_{550} time series is episodic but stable in the long term. Monthly medians broaden in late spring and summer when pollen and dust are frequent, yet the central tendency remains flat; the fitted trend is not different from zero (slope: -0.02 ± 0.01 $m^2g^{-1}yr^{-1}$; relative trend: -1.13 ± 0.94 $\%yr^{-1}$; Fig. 2(d); Table 3). A recurrent winter-high/summer-low seasonal cycle persists throughout the record and no step change is evident across the 2018 instrument transition. Event–non-event differences in distribution are confirmed with a one-sided Mann–Whitney U test (Section 4.2), indicating that episodes widen the spread but do not impose a drift. For context, PM_{10} and PM_1 show larger MSC_{550} magnitudes yet the same time-series behaviour, that is, short-term variability around a level baseline, with trends statistically indistinguishable from 0 (PM_{10} slope: 3.70

x 10^{-3} ± 0.02 $m^2g^{-1}yr^{-1}$; PM_{10} relative trend: 0.15 ± 0.64 $\%yr^{-1}$; PM_1 slope: 1.54 x 10^{-3} ± 0.02 $m^2g^{-1}yr^{-1}$; PM_1 relative trend: 0.05 ± 0.54 $\%yr^{-1}$; Figures. S3(d) and S4(d); Tables S3(g) and S4(g)). The MSC_{550} represents the scattering efficiency of aerosol particles per unit mass and is a key parameter in assessing their radiative effects. The PM_{10} aerosol particles exhibit an upward trend, albeit statistically significant, with a slope of 0.04 ± 1.19 × 10^{-2} $m^2g^{-1}yr^{-1}$; 1.65 ± 0.45 $\%yr^{-1}$ (Figure S3(d); Table S3(g)), reinforcing the role of scattering aerosols across different size fractions. The observed changes may be linked to long-term reductions in anthropogenic emissions and variations in aerosol sources, which influence particle composition and optical properties (Ehn et al., 2014; Pandolfi et al., 2014). Additionally, shifts in aerosol size distribution could contribute to the increasing MSC_{550} trend for the PM_{10} aerosol particles, as larger particles scatter light less efficiently per unit mass compared to the PM_1 aerosol particles.

Even the PM_1 aerosol particles exhibits a similarly increasing trend in MSC_{550}, with a trend of 0.05 ± 1.21 × 10^{-2} $m^2g^{-1}yr^{-1}$; 1.46 ± 0.37 $\%yr^{-1}$ (Figure S4(d); Table S4(g)). This increase indicates that fine-mode aerosol particles, which are primarily composed of secondary organic aerosols and sulfates, have experienced a more or less similar trend in their scattering efficiency per unit mass. This trend may reflect changes in precursor emissions, aerosol aging processes, or chemical transformations in the atmosphere. Additionally, reductions in sulfate mass fractions within PM_1 could lead to a lower MSC_{550}, as sulfates are highly efficient scatterers (Pandolfi et al., 2014; Seinfeld & Pandis, 2016). Given the importance of scattering aerosols in modulating radiative forcing, long-term observations of MSC_{550} remain essential for understanding aerosol–radiation interactions and improving climate model predictions.

3.3.5 Mass absorption coefficient (MAC_{520})

For PM_{1-10}, MAC_{520} decreases significantly (slope: $-2.77 \times 10^{-3} \pm 9.04 \times 10^{-4}$ $m^2g^{-1}yr^{-1}$; relative trend: −3.97 ± 1.30 % yr^{-1}; Figure 4e; Table 3(h)). PM_{10} and PM_1 exhibit no significant trends (PM_{10}: $-9.30 \times 10^{-3} \pm 3.29 \times 10^{-3}$ $m^2g^{-1}yr^{-1}$, Table S3(h); PM_1: $-0.01 \pm 5.08 \times 10^{-3}$ $m^2g^{-1}yr^{-1}$, Table S4(h)). Values use the pseudo-daily means defined in Section 2.3. In Figure S10, PM_{10} is shown in panels (a) AE31 (2010–2017) and (b) AE33 (2018–2022), PM_1 in (c) AE31 (2010–2017) and (d) AE33 (2018–2022), and PM_{1-10} in (e) AE31 (2010–2017) and (f) AE33 (2018–2022). A positive instrument-related offset is evident for AE33 relative to AE31, which is most pronounced for the PM_{10} and PM_{1-10} aerosol particles and is consistent with reduced filter-loading bias due to the AE33 dual-spot correction. This positive offset makes any 2010–2022 decrease appear smaller, so the observed PM_{1-10} decline in the MAC_{520} is not caused by the instrument change (Bond et al., 1999; Weingartner et al., 2003; Virkkula, 2010; Drinovec et al., 2015; Zotter et al., 2017). The MAC_{520} for PM_{1-10} aerosol particles exhibits a statistically significant decreasing trend, with a slope of -2.66 × 10^{-3} ± 6.69 × 10^{-4} $m^2g^{-1}yr^{-1}$; -3.47 ± 0.87 $\%yr^{-1}$ (Figure 2(e); Table 3(h)). This decline suggests a reduction in the light-absorbing efficiency per unit mass, likely driven by decreasing BC contributions or chemical transformations in absorbing aerosol particles (Bergstrom et al., 2007; Lack & Cappa, 2010). The decreasing trend is consistent with long-term reductions in anthropogenic emissions, although the observed MAC_{520} trend in the PM_{1-10} fraction raises questions regarding its underlying causes. While the MAC_{520} is defined for all aerosol size fractions, its variability in PM_{1-10} aerosol particles is

~~influenced by both black carbon presence and the potential effects of measurement uncertainties. This raises the possibility that either (1) BC-containing particles contribute to the MAC_{520} in the coarse mode or (2) measurement artifacts are affecting the trend. A similar decreasing trend in PM_{10} (Figure S3(e)) suggests that changes in absorbing components are affecting multiple size fractions, while the weaker trend in PM_1 (Figure S4(e)) aligns with the persistence of BC in finer aerosols.~~

~~A potential contributing factor to this trend is the transition from Aethalometer AE31 to AE33 in March 2018. This instrument change may have introduced a discontinuity in the MAC_{520} values due to differences in filter-loading correction and multiple-scattering adjustments (Drinovec et al., 2015). Unlike AE31, which requires post-processing corrections, AE33 applies a real-time dual-spot correction method, known to yield systematically lower absorption values (Zotter et al., 2017). This suggests that part of the observed decline in the MAC_{520} may be attributed to instrument-related biases rather than actual atmospheric changes.~~

3.4 Seasonal variability of the extensive properties

The $\sigma_{abs,520}$ follows a strong seasonal cycle, with the highest values observed in winter (December, January and February) due to increased BC emissions from residential wood burning (Kukkonen et al., 2020; Pandolfi et al., 2014) in Finland. Additionally, the lower PBL during winter reduces vertical dispersion, leading to higher near-surface aerosol concentrations due to thermal inversion (Petäjä et al., 2016). These findings are consistent with Hyvärinen et al. (2011), which reported elevated BC concentrations in Finland during winter, primarily due to increased heating emissions and stable atmospheric conditions. In contrast, $\sigma_{abs,520}$ values are lower in May, June and July, mainly due to reduced heating emissions and an elevated PBL, which enhances aerosol dispersion (Arola et al., 2011). It is also possible that the correction algorithms were not entirely sufficient to minimize the sensitivity of the absorption measurements to the accumulation of aerosol particles on the filter. Meanwhile, the $\sigma_{sca,550}$ for PM_{10}, PM_1, and PM_{1-10} also exhibits distinct seasonal variability, with the highest values occurring in summer (June, July and August) and the lowest in April and October (Figures S5(a), S6(a) and 3(a)). The summer peak is attributed to increased emissions of BVOCs and enhanced SOA formation, consistent with findings that SOA dominates aerosol composition in boreal regions during summer (Kourtchev et al., 2016; Tunved et al., 2006).

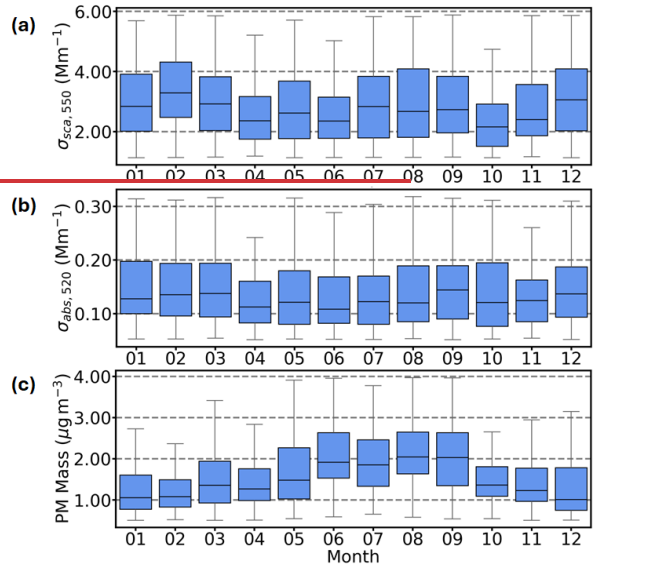

961

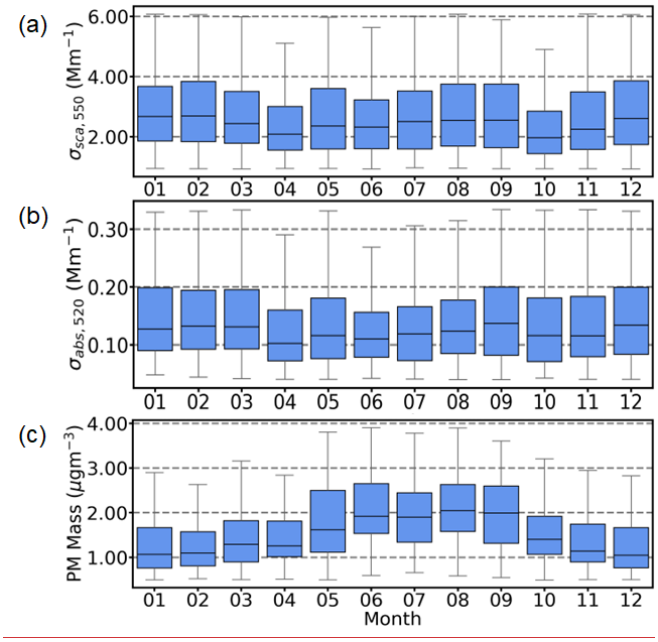

962

963

964 **Figure 3.** Monthly variations of aerosol optical properties for the $PM_{1\text{-}10}$ aerosol particles from October 2010 to
965 October 2022 (a) $\sigma_{sca,550}$, (b) $\sigma_{abs,520}$, and (c) PM mass. Box plots represent the interquartile range, with the first

horizontal line showing the 25th percentile, the middle line showing the median (50th percentile), and the third horizontal line showing the 75th percentile. Whiskers extend to the 10th and 90th percentiles.

The April and October minima are linked to reduced household heating emissions in spring and their delayed onset in autumn, along with weaker long-range transport contributions during these transitional months (Hienola et al., 2013). The seasonal variation in PM mass at Hyytiälä, as shown in Figure S5(c) for PM_{10}**,** Figure S6(c) for PM_1 and Figure 3(c) for $PM_{1–10}$ aerosol particles, further highlights differences between aerosol size fractions. PM_1 mass concentrations increase significantly during June–August, coinciding with enhanced SOA production, as indicated by the concurrent rise in $\sigma_{sca,550}$ for PM_1 Figures S6(a). These trends align with long-term aerosol observations in Finland (Luoma et al., 2019), which report similar seasonal variations in PM mass and composition. Meanwhile, PM_{10} and $PM_{1–10}$ mass also show seasonal variability, increasing in May, coinciding with the peak in birch pollen emissions (Yli-Panula et al., 2009). Additionally, June and July peaks in these fractions may indicate long-range transported mineral dust from the Aral-Caspian and Middle Eastern regions (Varga et al., 2023). Seasonal variations in atmospheric transport and aerosol sources further contribute to these trends, with summer months favoring photochemical activity and secondary aerosol formation, while winter remains dominated by local primary emissions.

3.5 Seasonal variability of the intensive properties

The seasonal variability of intensive aerosol properties at Hyytiälä provides insight into the sources and composition of PM_{10} and PM_{1-10} aerosol particles. Figures 4(d) and 4(e) illustrate the monthly variations of the MAC_{520} and the MSC_{550}. MAC_{520} peaks in winter due to increased emissions from biomass burning and residential heating, as shown by Heikkinen et al. (2021) and Virkkula et al. (2011). Reduced boundary-layer heights further enhance BC accumulation, leading to higher MAC_{520} values. Conversely, the MAC_{520} declines in summer due to the dominance of SOA from biogenic sources (Äijälä et al., 2019). Organic aerosols scatter more light than they absorb, reducing the MAC_{520} values. The seasonal minimum in the imaginary part of the refractive index further indicates lower absorption capacity in summer, reinforcing the shift toward scattering-dominated aerosols (Virkkula et al., 2011).

The MSC_{550} follows a distinct seasonal cycle, with peak values in winter (Figure 4(d)). The prevalence of fine-mode PM_1 particles, primarily from residential heating, enhances light scattering (Hellén et al., 2008). Although BC is present, the aerosol mixture includes significant amounts of scattering species such as SOA and sulfates, leading to high MSC_{550} values (Seinfeld & Pandis, 2016). Despite an increase in the *PM mass* in summer, MSC_{550} declines due to a shift toward larger particles that scatter light less efficiently per unit mass (Tunved et al., 2006). The seasonal reduction in the MSC_{550} aligns with greater contributions from pollen, mineral dust, and sea salt aerosols in the PM_{1-10} fraction, altering the aerosol size distribution (Latimer & Martin, 2019). These shifts emphasize the importance of size-dependent scattering efficiency in shaping seasonal aerosol optical properties.

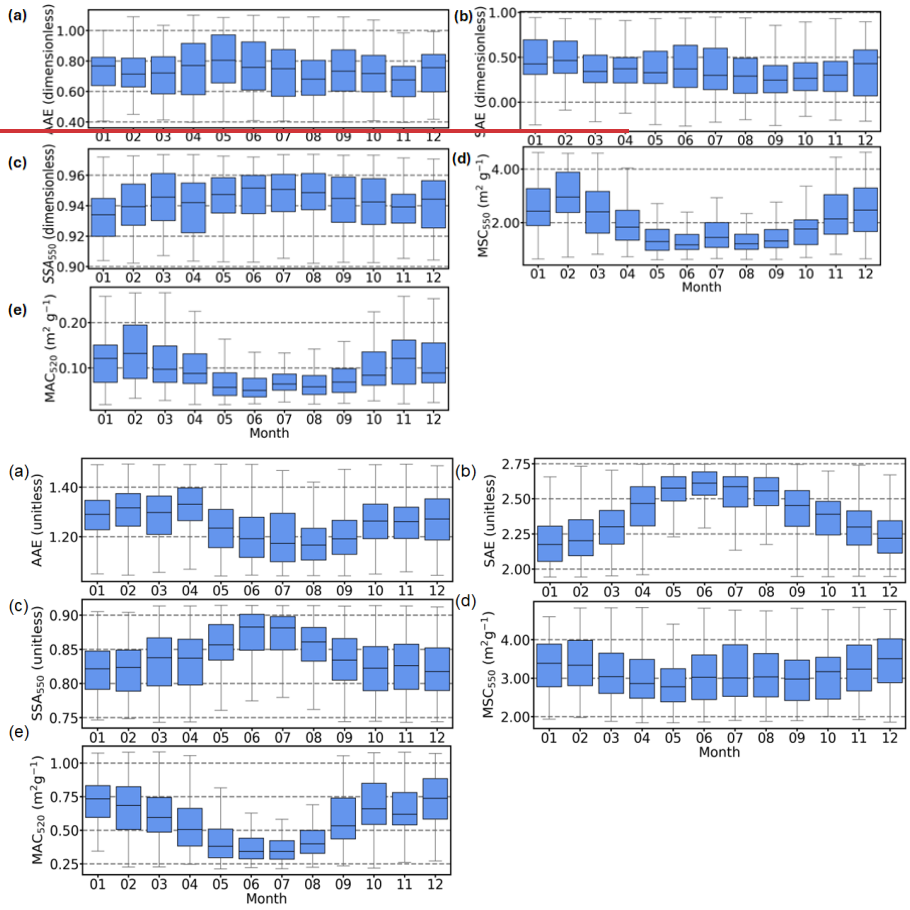

Figure 4. Monthly variations of aerosol optical properties for the $PM_{1\text{-}10}$ aerosol particles from October 2010 to October 2022 (a) AAE, (b) SAE, (c) SSA_{550}, (d) MSC_{550} and (e) MAC_{520}. Box plots represent the interquartile range, with the first horizontal line showing the 25th percentile, the middle line showing the median (50th percentile), and the third horizontal line showing the 75th percentile. Whiskers extend to the 10th and 90th percentiles.

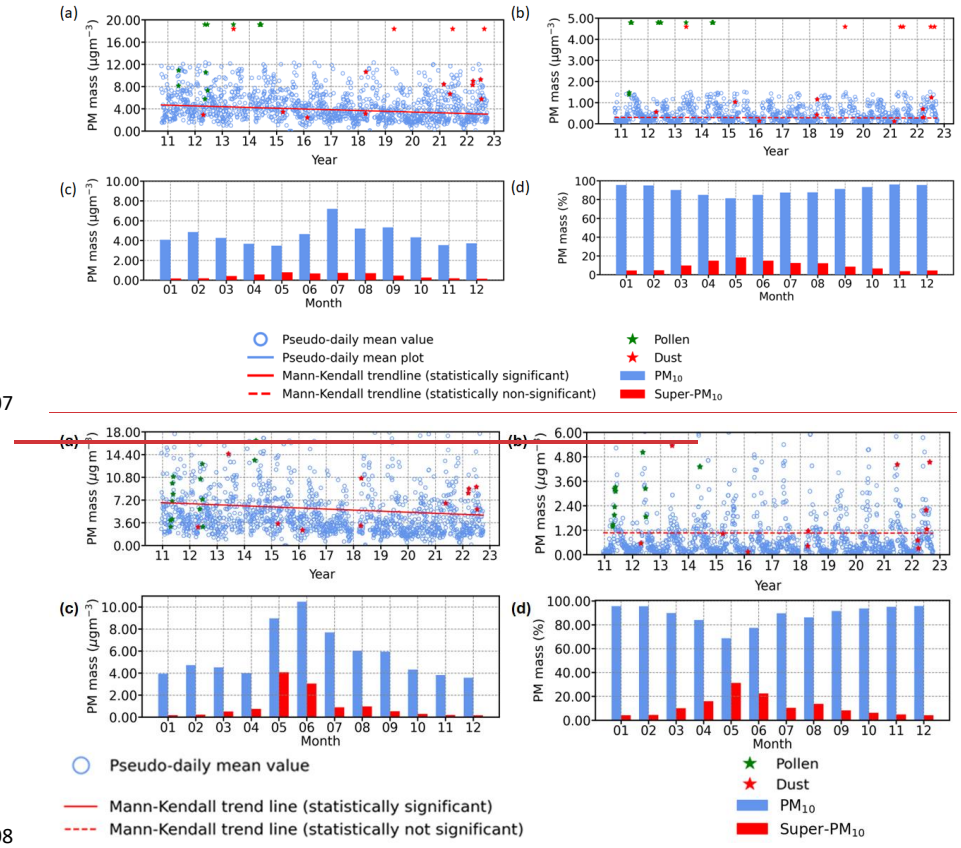

Figure 5. Temporal trend comparisons of PM mass in (a) PM_{10}, (b) super-PM_{10} aerosol particles and seasonal variation comparisons of PM_{10} and super-PM_{10} aerosol particles in terms of (c) PM mass concentration and (d) PM mass fraction.

The $PM_{1\text{-}10}$ fraction significantly influences seasonal aerosol dynamics, particularly in spring and summer when pollen and mineral dust events contribute to coarse-mode aerosol mass. However, optical measurements in this study are constrained by the PM_{10} inlet, excluding particles larger than 10 μm. Figure 5 quantifies this missing PM fraction, showing substantial coarse-mode mass is unaccounted for, especially during episodic events. The seasonal increase in $PM_{1\text{-}10}$ and PM_{10} mass suggests coarse-mode aerosols dominate specific periods, yet their optical contributions remain uncertain. Complementary measurement techniques are needed to capture the full size distribution of coarse-mode particles and improve the representation of their optical properties. The exclusion of super-PM_{10} from optical instruments introduces uncertainties in radiative forcing assessments, underscoring the necessity of including larger particles in aerosol characterization.

Pseudo-daily peaks in super-PM_{10} mass (Figure 5) indicate that episodic events, such as pollen and dust outbreaks, significantly impact aerosol optical properties. These events contribute to short-term fluctuations in the MAC_{520} and the MSC_{550}, reflecting shifts in aerosol composition and size distribution. The variability of super-PM_{10} mass suggests coarse-mode particles play a crucial role in modifying scattering and absorption properties, further complicating aerosol–radiation interactions. Without direct optical measurements of these particles, their contribution to aerosol optical closure remains uncertain. The high mass fraction of super-PM_{10} during episodic events suggests that excluding these particles leads to an underestimation of coarse-mode aerosol influences in climate models. The seasonal trends and episodic peaks observed in Figures 4 and 5, respectively emphasize the need for improved measurement techniques and better parameterization of coarse-mode aerosols in radiative forcing assessments.

4. Role of episodic variability

4.1 Optical and mass properties of PM_{10} aerosol particles at Hyytiälä: Episodic events and long-term trends

The optical and mass properties of PM_{10} aerosol particles at Hyytiälä exhibit variability influenced by episodic events and long-term trends. To classify the dominant aerosol types, we applied the framework by Cazorla et al. (2013), which utilizes the *SAE* and the *AAE*, as shown in Figure 6.

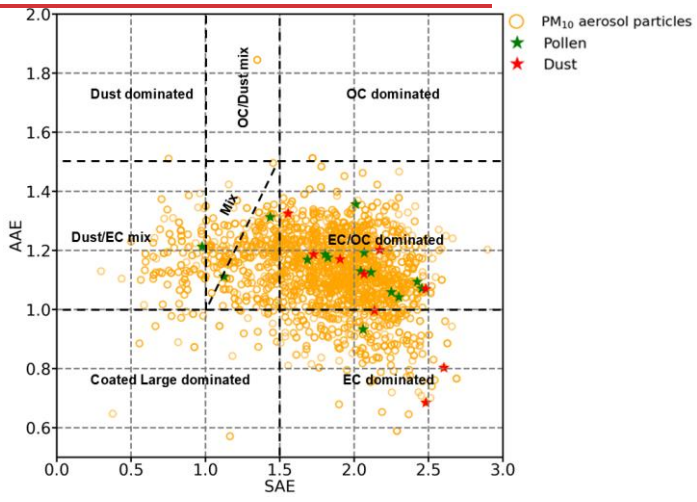

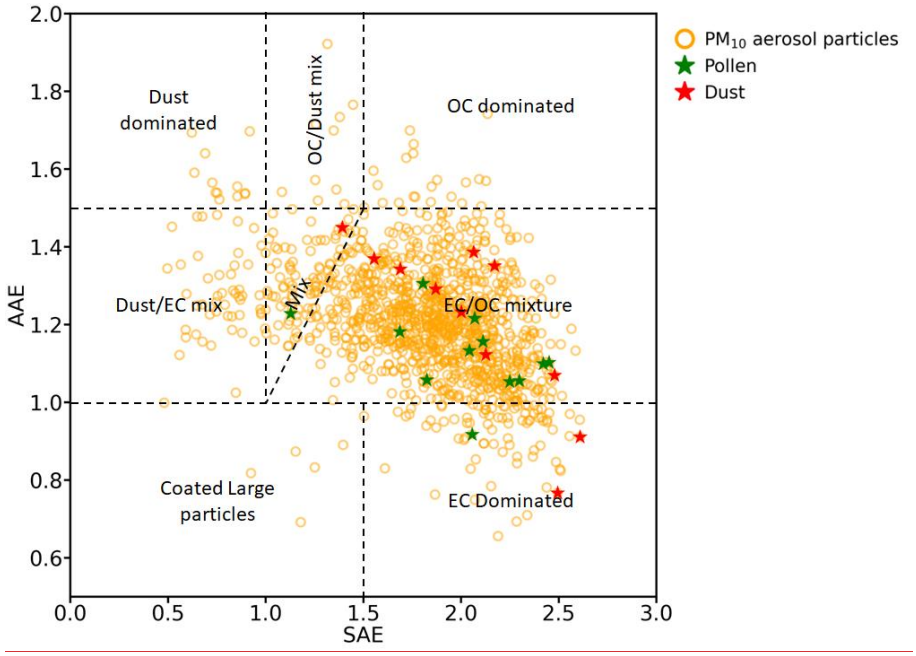

Figure 6. Aerosol classification matrix for the PM_{10} aerosol particles.

Figure 6 presents the aerosol classification for PM_{10} particles, as PM_{10} encompasses both PM_1 and $PM_{1\text{-}10}$ aerosols, providing a broader representation of aerosol interactions. The data show that PM_{10} particles predominantly fall within the *'EC/OC-dominated'* and *'Dust/EC-dominated'* regions, indicating contributions from combustion-derived BC, SOA, and aged dust.

Pollen and dust events appear sporadically, clustering in moderate to high *AAE* and *SAE* regions, reinforcing their episodic nature. These events introduce short-term fluctuations in aerosol properties but do not significantly alter the long-term classification. Dust events cluster near the *'Dust/EC-dominated'* region, suggesting interactions between long-range transported dust and combustion aerosols. Pollen events align with higher *SAE* (~1.5–2), indicating smaller particles with strong scattering properties.

Despite episodic variability, the dominant aerosol classification remains stable, with PM_{10} aerosols primarily linked to EC/OC sources and aged dust.

Table S3 summarizes the classification scheme used in this study, differentiating aerosol types based on their optical properties:

(1) High *SAE* (>1.5) and low *AAE* (~1): BC-dominated aerosols from fossil fuel combustion and biomass burning.

(2) High *AAE* (>2) and low *SAE* (<1): Mineral dust, often associated with long-range transport.

(3) Intermediate *AAE* (1–2) and *SAE* (~1): Aged dust mixed with BC, indicative of interactions between transported dust and combustion aerosols.

Table 3. Summary of aerosol classifications in Figure 6.

Region in Figure 6	AAE	SAE	Size	Aerosol classification	Supporting studies
Dust Dominated	>2	<1	Coarse (>2.5 μm)	Mineral dust (e.g., desert regions)	Cazorla et al. (2013): *AAE* ~2.5, *SAE* ~0.5. Russell et al. (2010): Dust, coarse mode, high *AAE*. Malm and Hand (2007): Dust from desert regions with low scattering efficiency.
Dust/EC Dominated	~1–2	~1	Mixed (fine + coarse)	Dust mixed with aged BC	Cazorla et al. (2013): Mixed values for overlapping dust/black carbon. Clarke et al. (2007): Combustion aerosols interacting with dust.
EC Dominated	~1	>1.5	Fine (<1 μm)	Fossil fuel combustion (i.e. BC)	Schuster et al. (2006): *AAE* ~1 for BC. Clarke et al. (2007): *SAE* >1.5 for fine combustion aerosols. Sheridan and Ogren (1999): BC classification with low *AAE*.
OC Dominated	1.5–2	1–1.5	Fine to accumulation mode	Biomass burning, SOA	Cazorla et al. (2013): *AAE* ~1.8 for OC, moderate *SAE*. Russell et al. (2010): *AAE* 1.5–2 linked to OC. Malm and Hand (2007): OC from regional biomass burning or SOA formation.
Coated Large Dominated	<0	<0.5	Mixed/coarse	Aged aerosols, sulfate coating on dust	Malm and Hand (2007): Sulfate coating reduces *SAE* and *AAE*. Clarke et al. (2007): Coated particles with low *SAE*.

					Sheridan and Ogren (1999): Mixed aerosols with coatings.
Dust/OC or EC/OC Mixed	1–1.5	~1	Mixed (fine + coarse)	Mixed sources: urban, industrial, or forest	Cazorla et al. (2013): Mixed *AAE/SAE* values for overlapping sources. Clarke et al. (2007): Mixing of dust and pollution aerosols in urban environments. Malm and Hand (2007): Regional mixing.

4.2 Episodic and long-term variability: One-sided Mann-Whitney U test

To assess the impact of episodic events (i.e., pollen and dust) on aerosol properties, a one-sided Mann-Whitney U test was conducted. This non-parametric statistical test is particularly suited for comparing two independent datasets without assuming normality, making it effective for aerosol optical property distributions, which often exhibit non-Gaussian behavior due to episodic influences.

The dataset was categorized into:

(a) Observations including pollen and/or dust events

(b) Observations excluding these events

Pollen events were identified using cascade impactor filter records. If the PM_{10} filters contained pollen, the corresponding PM_{1-10} fraction was also assumed to contain pollen.

Dust events were identified based on time periods from Varga et al. (2023), cross-referenced with aerosol optical and mass data from Hyytiälä.

Table 4. One-sided Mann-Whitney U-test results for the aerosol optical and mass properties in the presence of pollen and/or dust events for the $PM_{1–10}$ aerosol particles

Variable	Number of data points (pollen and/or dust events)	Number of data points (excluding pollen and /or dust events)	U-statistic	p-value	Statistical significance	Trend
$\sigma_{abs,520}$	2329	12083336	17442513 94	0.040.56	YesNo	DecreasingNo trend
$\sigma_{sca,550}$	2830	14463914	28653 79862	1.64 x 10^{-4} 6.63 x 10^{-4}	YesYes	DecreasingIncreasing
PM mass	3036	15333626	39156 94548	4.08 x 10^{-11} 3.51 x 10^{-6}	YesYes	DecreasingIncreasing
AAE	2329	11823254	14692 66718	0.511.21 x 10^{-4}	NoYes	No trendIncreasing
SAE	2830	14413880	21013 52785	0.710.38	NoNo	No trendNo trend
SSA_{550}	2123	11723174	12977 28940	0.678.65 x 10^{-2}	NoNo	No trendNo trend
MAC_{520}	2329	11792990	65373 1641	2.06 x 10^{-5} 1.22 x 10^{-2}	YesYes	DecreasingDecreasing
MSC_{550}	2830	14133515	10798 38484	3.79 x 10^{-5} 1.07 x 10^{-2}	YesYes	DecreasingDecreasing

A Mann–Whitney U test (one-sided) shows that $\sigma_{sca,550}$ (n = 28 pseudo-daily means) and *PM mass* (n = 30) are higher during pollen/dust events than during non-event periods *(event median > non-event median; p-value ≤ 0.05)*. MAC_{520} (n = 23) is lower during events *(event median < non-event median; p-value ≤ 0.05)*; MSC_{550} (n = 28) also differs significantly, and $\sigma_{abs,520}$ (n = 23) shows a weaker but significant difference. SSA_{550} (n = 21), *AAE* (n = 23), and *SAE* (n = 28) show no significant differences. PM_{10} mostly scatters light, but mineral dust in this size range can also absorb (Adebiyi et al., 2023).

Trends were estimated with a modified Theil–Sen slope and significance was tested with the Hamed & Rao (1998) autocorrelation-corrected Mann–Kendall test. The MAC_{520} decreases significantly *(p-value ≤ 0.05)*, while SSA_{550}, *AAE* and *SAE* show no trend *(p > 0.05)*; no other trends are claimed. σ_{sca} has been corrected for angular truncation and non-ideal angular response; some uncertainty remains because the correction depends on particle size distribution and refractive index (Anderson & Ogren, 1998; Müller et al., 2011). Filter-based absorption can retain

residual multiple-scattering and loading artifacts that bias σ_{abs} high (and thus MAC) (Weingartner et al., 2003; Bond et al., 1999; Ogren, 2010; Virkkula, 2010).

We show PM_{10} because it includes both PM_1 and $PM_{1–10}$ and the optics use a PM_{10} inlet (particles > 10 µm excluded). The data cluster mainly in the *EC/OC mixture* and *Dust/EC mix* regions, with few points in *Dust dominated* and *OC/Dust mix*. We therefore base interpretation on the better-sampled mixed regimes and separate episodic events from longer-term behavior (Adebiyi et al., 2023; Che et al., 2018), consistent with boreal observations of SOA-dominated backgrounds and mixed BC–organic conditions (Virkkula et al., 2011; Hyvärinen et al., 2011).~~Table 4 summarizes the statistical results. Statistically significant increases in $\sigma_{sca,550}$ (30 pseudo-daily mean values) were observed during identified pollen and/or dust events relative to periods without such events, indicating enhanced contributions from PM_{1-10} particles to aerosol scattering.~~

~~Conversely, significant decrease in MAC_{520} (29 pseudo-daily mean values) suggest reductions in absorbing components and a shift toward smaller, more scattering aerosols. While PM_{10} particles primarily scatter light, mineral dust within this size range can also absorb radiation, influencing aerosol radiative properties (Adebiyi et al., 2023).~~

~~No significant trends were detected for SSA_{550} (23 pseudo-daily mean values), AAE (29 pseudo-daily mean values) or SAE (30 psudo-daily mean values). However, MAC_{520} exhibited a significant decreasing trend (29 psudo-daily mean values), suggesting a declining contribution from black carbon and other absorbing components. The stable SSA_{550} values, combined with declining MAC_{520}, indicate a shift toward aerosols with higher scattering-to-absorption ratios, likely due to increased sulfate or organic aerosol contributions.~~

~~Intensive properties also show variability during dust transport events, emphasizing the need to differentiate episodic contributions from long-term trends when interpreting radiative forcing estimates (Adebiyi et al., 2023; Che et al., 2018).~~

~~The aerosol classifications and trends observed in this study align with prior boreal aerosol research:~~

~~1. Virkkula et al. (2011) found that secondary organic aerosols (SOA) dominate boreal environments, with episodic pollen and dust events temporarily increasing coarse-mode contributions, aligning with the 'Dust-dominated' and 'Dust/EC-dominated' regions.~~

~~2. Hyvärinen et al. (2011) reported that long-range transported BC interacts with local aerosols, producing intermediate AAE values (~1–2), characteristic of the 'Dust/EC-dominated' region.~~

~~3. Laing et al. (2016) emphasized the role of SOA and organic carbon aerosols from biomass burning in boreal forests, corresponding to the 'OC-dominated' classification (AAE 1.5–2, SAE 1–1.5).~~

~~Coarse-mode aerosol measurements are affected by instrument-specific errors, such as angular truncation in nephelometers and artifacts in filter-based absorption techniques (Müller et al., 2011; Sheridan & Ogren, 1999). These uncertainties should be considered in climate models to improve estimates of aerosol–radiation interactions.~~

5. Summary and conclusions

This study provides new insights into the long-term evolution of aerosol optical properties and PM mass at the SMEAR II station in Hyytiälä, southern Finland, over the past 12 years. A significant decrease in extensive aerosol properties in PM_{10} aerosols suggests a shift in size distribution and chemical composition, likely driven by declining anthropogenic emissions, including SO_2, across northern Europe (Tørseth et al., 2012; Zieger et al., 2010). Seasonal patterns show that absorbing aerosols peak in winter due to biomass burning and residential heating, while scattering aerosols peak in summer, influenced by biogenic SOA formation and episodic pollen and dust events. These findings reinforce previous research on boreal aerosol processes and highlight the complex interactions between anthropogenic and natural aerosol sources at this site.

To address the challenge of incomplete optical closure, this study examines the role of supermicron aerosol particles across multiple seasons. The first-ever quantification of super-PM_{10} particles at Hyytiälä underscores their role in aerosol scattering and absorption processes, contributing to uncertainties in aerosol–radiation interactions. Statistical analysis revealed that pollen and dust events significantly affected five of the eight $PM_{1\text{-}10}$ aerosol optical and mass-related properties examined. The observed trends in MAC_{520} and MSC_{550} suggest changes in aerosol composition and size distribution, which must be considered in radiative forcing assessments. Future work should improve the representation of supermicron aerosols in climate models by leveraging advanced analytical techniques, such as machine learning-based aerosol classification (Schuster et al., 2006) and integrating multi-platform observational datasets to reduce uncertainties.

Code/Data availability

The codes and data are available can be found at https://doi.org/10.5281/zenodo.15213383 (Banerji et al., 2025).

Field Code Changed

Author contributions

SB, KL and TP conceptualized the study. SB performed the data analysis. IY and LA contributed to the collection of data at SMEAR II. SB wrote the original draft and prepared the manuscript with input from KL. KL, IY, VMK and TP contributed to the review and revision of the manuscript, including the final edits. TP provided overall supervision and secured funding.

Competing interests

One of the co-authors is a member of the editorial board of *Atmospheric Chemistry and Physics*. This co-author had no involvement in the peer-review or editorial decision-making process for this manuscript. The authors declare no other competing interests.

Acknowledgements

The funding from ACTRIS-Finland host organizations University of Helsinki (UH) and INAR RI/ ACTRIS-FI 2020-2024 grant no. 328616, INAR RI 2022-2025 grant no. 345510 (UH), and the ACCC (Atmosphere and Climate Competence Center) Flagship funding by the Research Council of Finland (grant no. 337549 (UH) are gratefully acknowledged.

Support of the European Commission via non-CO_2 forcers and their climate, weather, air quality and health impacts (FOCI, project number 101056783) is gratefully acknowledged.

During the preparation of this work the authors used ChatGPT to improve the readability of certain sections. After using this tool, the authors reviewed and edited the content as needed and take full responsibility for the content of the manuscript.

References

Adebiyi, A., Kok, J. F., Murray, B. J., Ryder, C. L., Stuut, J.-B. W., Kahn, R. A., Knippertz, P., Formenti, P., Mahowald, N. M., Pérez García-Pando, C., Klose, M., Ansmann, A., Samset, B. H., Ito, A., Balkanski, Y., Di Biagio, C., Romanias, M. N., Huang, Y., & Meng, J. (2023). A review of coarse mineral dust in the Earth system. *Aeolian Research*, *60*, 100849. https://doi.org/https://doi.org/10.1016/j.aeolia.2022.100849

Äijälä, M., Daellenbach, K. R., Canonaco, F., Heikkinen, L., Junninen, H., Petäjä, T., Kulmala, M., Prévôt, A. S. H., & Ehn, M. (2019). Constructing a data-driven receptor model for organic and inorganic aerosol – a synthesis analysis of eight mass spectrometric data sets from a boreal forest site. *Atmospheric Chemistry and Physics*, *19*(6), 3645-3672. https://doi.org/10.5194/acp-19-3645-2019

Anderson, T. L., Covert, D. S., Marshall, S. F., Laucks, M. L., Charlson, R. J., Waggoner, A. P., Ogren, J. A., Caldow, R., Holm, R. L., Quant, F. R., Sem, G. J., Wiedensohler, A., Ahlquist, N. A., & Bates, T. S. (1996). Performance Characteristics of a High-Sensitivity, Three-Wavelength, Total Scatter/Backscatter Nephelometer. *Journal of Atmospheric and Oceanic Technology*, *13*(5), 967-986. https://doi.org/https://doi.org/10.1175/1520-0426(1996)013

Anderson, T. L., & Ogren, J. A. (1998). Determining Aerosol Radiative Properties Using the TSI 3563 Integrating Nephelometer. *Aerosol Science and Technology*, *29*(1), 57-69. https://doi.org/10.1080/02786829808965551

Andreae, M. O., & Gelencsér, A. (2006). Black carbon or brown carbon? The nature of light-absorbing carbonaceous aerosols. *Atmos. Chem. Phys.*, *6*(10), 3131-3148. https://doi.org/10.5194/acp-6-3131-2006

Arnott, W. P., K. Hamasha, H. Moosmüller, P. J. Sheridan, and J. A. Ogren (2005). Towards Aerosol Light-Absorption Measurements with a 7-Wavelength Aethalometer: Evaluation with a Photoacoustic Instrument and 3-Wavelength Nephelometer, *Aerosol Sci. Technol.*, 39, 17-29. doi.org/10.1080/027868290901972

Arola, A., Schuster, G., Myhre, G., Kazadzis, S., Dey, S., & Tripathi, S. N. (2011). Inferring absorbing organic carbon content from AERONET data. *Atmospheric Chemistry and Physics*, *11*(1), 215-225. https://doi.org/10.5194/acp-11-215-2011

Backman, J., Schmeisser, L., Virkkula, A., Ogren, J. A., Asmi, E., Starkweather, S., Sharma, S., Eleftheriadis, K., Uttal, T., Jefferson, A., Bergin, M., Makshtas, A., Tunved, P., & Fiebig, M. (2017). On Aethalometer measurement uncertainties and an instrument correction factor for the Arctic. *Atmos. Meas. Tech.*, *10*(12), 5039-5062. https://doi.org/10.5194/amt-10-5039-2017

Bali, K., Banerji, S., Campbell, J. R., Bhakta, A. V., Chen, L. W. A., Holmes, C. D., & Mao, J. (2024). Measurements of brown carbon and its optical properties from boreal forest fires in Alaska summer. *Atmospheric Environment*, *324*, 120436-120436. https://doi.org/https://doi.org/10.1016/j.atmosenv.2024.120436

Banerji, S., Luoma, K., Ylivinkka, I., Ahonen, L., Kerminen, V.-M., & Petäjä, T. (2025). *Data for "Measurement Report: Optical properties of supermicron aerosol particles in a boreal environment", Zenodo [data set]* https://doi.org/https://doi.org/10.5281/zenodo.15213383

Bates, T. S., Quinn, P. K., Coffman, D. J., Johnson, J. E., & Middlebrook, A. M. (2005). Dominance of organic aerosols in the marine boundary layer over the Gulf of Maine during NEAQS 2002 and their role in aerosol light scattering. *Journal of Geophysical Research: Atmospheres*, *110*(D18). https://doi.org/https://doi.org/10.1029/2005JD005797

Bergstrom, R. W., Pilewskie, P., Russell, P. B., Redemann, J., Bond, T. C., Quinn, P. K., & Sierau, B. (2007). Spectral absorption properties of atmospheric aerosols. *Atmos. Chem. Phys.*, *7*(23), 5937-5943. https://doi.org/10.5194/acp-7-5937-2007

Bernardoni, V., Ferrero, L., Bolzacchini, E., Forello, A. C., Gregorič, A., Massabò, D., Močnik, G., Prati, P., Rigler, M., Santagostini, L., Soldan, F., Valentini, S., Valli, G., & Vecchi, R. (2021). Determination of Aethalometer multiple-scattering enhancement parameters and impact on source apportionment during the winter 2017/18 EMEP/ACTRIS/COLOSSAL campaign in Milan. *Atmos. Meas. Tech.*, *14*(4), 2919-2940. https://doi.org/10.5194/amt-14-2919-2021

Berner, A., & Luerzer, C. (1980). Mass size distributions of traffic aerosols at Vienna. *The Journal of Physical Chemistry*, *84*(16), 2079-2083. https://doi.org/10.1021/j100453a016

Bond, T. C., Anderson, T. L., & Campbell, D. (1999). Calibration and intercomparison of filter-based measurements of visible light absorption by aerosols. *Aerosol Science and Technology*, 30(6), 582–600. https://doi.org/10.1080/027868299304435

Bond, T. C., & Bergstrom, R. W. (2006). Light Absorption by Carbonaceous Particles: An Investigative Review. *Aerosol Science and Technology*, *40*(1), 27-67. https://doi.org/10.1080/02786820500421521

Bond, T. C., Doherty, S. J., Fahey, D. W., Forster, P. M., Berntsen, T., Deangelo, B. J., Flanner, M. G., Ghan, S., Kärcher, B., Koch, D., Kinne, S., Kondo, Y., Quinn, P. K., Sarofim, M. C., Schultz, M. G., Schulz, M., Venkataraman, C., Zhang, H., Zhang, S., . . . Zender, C. S. (2013). Bounding the role of black carbon in the climate system: A scientific assessment. *Journal of Geophysical Research Atmospheres*, *118*(11), 5380-5552. https://doi.org/10.1002/jgrd.50171

Boy, M. (2004). Overview of the field measurement campaign in Hyytiala, August 2001 in the frame of the EU project OSOA (vol 4, pg 657, 2004). *Atmospheric Chemistry and Physics*, *4*, 1739-1739. https://acp.copernicus.org/articles/4/657/2004/acp-4-657-2004.pdf

Brasseur, Z., Castarède, D., Thomson, E. S., Adams, M. P., Drossaart van Dusseldorp, S., Heikkilä, P., Korhonen, K., Lampilahti, J., Paramonov, M., Schneider, J., Vogel, F., Wu, Y., Abbatt, J. P. D., Atanasova, N. S., Bamford, D. H., Bertozzi, B., Boyer, M., Brus, D., Daily, M. I., . . . Duplissy, J. (2022). Measurement report: Introduction to the HyICE-2018 campaign for measurements of ice-nucleating particles and instrument inter-comparison in the Hyytiälä boreal forest. *Atmospheric Chemistry and Physics*, *22*(8), 5117-5145. https://doi.org/10.5194/acp-22-5117-2022

Brasseur, Z., Schneider, J., Lampilahti, J., Vakkari, V., & Sinclair, V. A. (2024). Vertical distribution of ice nucleating particles over the boreal forest of Hyytiälä , Finland. 11305-11332.

Cappa, C. D., Kolesar, K. R., Zhang, X., Atkinson, D. B., Pekour, M. S., Zaveri, R. A., Zelenyuk, A., & Zhang, Q. (2016). Understanding the optical properties of ambient sub-and supermicron particulate matter: Results from the CARES 2010 field study in northern California. *Atmospheric Chemistry and Physics*, *16*(10), 6511-6535. https://doi.org/10.5194/acp-16-6511-2016

Cazorla, A., Bahadur, R., Suski, K. J., Cahill, J. F., Chand, D., Schmid, B., Ramanathan, V., & Prather, K. A. (2013). Relating aerosol absorption due to soot, organic carbon, and dust to emission sources determined from in-situ chemical measurements. *Atmospheric Chemistry and Physics*, *13*(18), 9337-9350. https://doi.org/10.5194/acp-13-9337-2013

Che, H., Qi, B., Zhao, H., Xia, X., Eck, T. F., Goloub, P., Dubovik, O., Estelles, V., Cuevas-Agulló, E., Blarel, L., Wu, Y., Zhu, J., Du, R., Wang, Y., Wang, H., Gui, K., Yu, J., Zheng, Y., Sun, T., . . . Zhang, X. (2018). Aerosol optical properties and direct radiative forcing based on measurements from the China Aerosol Remote Sensing Network (CARSNET) in eastern China. *Atmos. Chem. Phys.*, *18*(1), 405-425. https://doi.org/10.5194/acp-18-405-2018

Collaud Coen, M., Andrews, E., Lastuey, A., Petkov Arsov, T., Backman, J., Brem, B. T., Bukowiecki, N., Couret, C., Eleftheriadis, K., Flentje, H., Fiebig, M., Gysel-Beer, M., Hand, J. L., Hoffer, A., Hooda, R., Hueglin, C., Joubert, W., Keywood, M., Eun Kim, J., . . . Laj, P. (2020). Multidecadal trend analysis of in situ aerosol radiative properties around the world. *Atmospheric Chemistry and Physics*, *20*(14), 8867-8908. https://doi.org/10.5194/acp-20-8867-2020

Collaud Coen, M., Weingartner, E., Apituley, A., Ceburnis, D., Fierz-Schmidhauser, R., Flentje, H., Henzing, J. S., Jennings, S. G., Moerman, M., Petzold, A., Schmid, O., & Baltensperger, U. (2010). Minimizing light

Formatted: Left

absorption measurement artifacts of the Aethalometer: evaluation of five correction algorithms. *Atmos. Meas. Tech.*, *3*(2), 457-474. https://doi.org/10.5194/amt-3-457-2010

Després, V. R., Huffman, J. A., Burrows, S. M., Hoose, C., Safatov, A. S., Buryak, G., Fröhlich-Nowoisky, J., Elbert, W., Andreae, M. O., Pöschl, U., & Jaenicke, R. (2012). Primary biological aerosol particles in the atmosphere: a review. *Tellus B: Chemical and Physical Meteorology*, *64*(1). https://doi.org/10.3402/tellusb.v64i0.15598

Drinovec, L., Močnik, G., Zotter, P., Prévôt, A. S. H., Ruckstuhl, C., Coz, E., Rupakheti, M., Sciare, J., Müller, T., Wiedensohler, A., & Hansen, A. D. A. (2015). The "dual-spot" Aethalometer: an improved measurement of aerosol black carbon with real-time loading compensation. *Atmos. Meas. Tech.*, *8*(5), 1965-1979. https://doi.org/10.5194/amt-8-1965-2015

Ehn, M., Thornton, J. A., Kleist, E., Sipilä, M., Junninen, H., Pullinen, I., Springer, M., Rubach, F., Tillmann, R., Lee, B., Lopez-Hilfiker, F., Andres, S., Acir, I.-H., Rissanen, M., Jokinen, T., Schobesberger, S., Kangasluoma, J., Kontkanen, J., Nieminen, T., . . . Mentel, T. F. (2014). A large source of low-volatility secondary organic aerosol. *Nature*, *506*(7489), 476-479. https://doi.org/10.1038/nature13032

Emerson, E. W., Hodshire, A. L., DeBolt, H. M., Bilsback, K. R., Pierce, J. R., McMeeking, G. R., & Farmer, D. K. (2020). Revisiting particle dry deposition and its role in radiative effect estimates. *Proceedings of the National Academy of Sciences*, *117*(42), 26076-26082. https://doi.org/10.1073/pnas.2014761117

Guenther, A., Karl, T., Harley, P., Wiedinmyer, C., Palmer, P. I., & Geron, C. (2006). Estimates of global terrestrial isoprene emissions using MEGAN (Model of Emissions of Gases and Aerosols from Nature). *Atmos. Chem. Phys.*, *6*(11), 3181-3210. https://doi.org/10.5194/acp-6-3181-2006

Hakola, H., Tarvainen, V., Laurila, T., Hiltunen, V., Hellén, H., & Keronen, P. (2003). Seasonal variation of VOC concentrations above a boreal coniferous forest. *Atmospheric Environment*, *37*(12), 1623-1634. https://doi.org/10.1016/s1352-2310(03)00014-1

Hallquist, M., Wenger, J. C., Baltensperger, U., Rudich, Y., Simpson, D., Claeys, M., Dommen, J., Donahue, N. M., George, C., Goldstein, A. H., Hamilton, J. F., Herrmann, H., Hoffmann, T., Iinuma, Y., Jang, M., Jenkin, M. E., Jimenez, J. L., Kiendler-Scharr, A., Maenhaut, W., . . . Wildt, J. (2009). The formation, properties and impact of secondary organic aerosol: current and emerging issues. *Atmos. Chem. Phys.*, *9*(14), 5155-5236. https://doi.org/10.5194/acp-9-5155-2009

Hamed, K. H., & Rao, A. R. (1998). A modified Mann–Kendall trend test for autocorrelated data. *Journal of Hydrology*, *204*(1–4), 182–196. https://doi.org/10.1016/S0022-1694(97)00125-X

Hari, P., & Kulmala, M. (2005). Station for Measuring Ecosystem-Atmosphere Relations (SMEAR II). *Boreal Environment Research*, *10*, 315-322. https://www.borenv.net/BER/archive/pdfs/ber10/ber10-315.pdf

Hari, P., Nikinmaa, E., Pohja, T., Siivola, E., Bäck, J., Vesala, T., & Kulmala, M. (2013). Station for measuring ecosystem-atmosphere relations: SMEAR. *Physical and Physiological Forest Ecology*, *9789400756*(October), 471-487. https://doi.org/10.1007/978-94-007-5603-8_9

Heikkinen, L., Äijälä, M., Daellenbach, K. R., Chen, G., Garmash, O., Aliaga, D., Graeffe, F., Räty, M., Luoma, K., Aalto, P., Kulmala, M., Petäjä, T., Worsnop, D., & Ehn, M. (2021). Eight years of sub-micrometre organic aerosol composition data from the boreal forest characterized using a machine-learning approach. *Atmospheric Chemistry and Physics*, *21*(13), 10081-10109. https://doi.org/10.5194/acp-21-10081-2021

Heikkinen, L., Äijälä, M., Riva, M., Luoma, K., Dällenbach, K., Aalto, J., Aalto, P., Aliaga, D., Aurela, M., Keskinen, H., Makkonen, U., Rantala, P., Kulmala, M., Petäjä, T., Worsnop, D., & Ehn, M. (2020). Long-term sub-micrometer aerosol chemical composition in the boreal forest: inter- and intra-annual variability. *Atmospheric Chemistry and Physics*, *20*(5), 3151-3180. https://doi.org/10.5194/acp-20-3151-2020

Heikkinen, L., Partridge, D. G., Blichner, S., Huang, W., Ranjan, R., Bowen, P., Tovazzi, E., Petäjä, T., Mohr, C., & Riipinen, I. (2024). Cloud response to co-condensation of water and organic vapors over the boreal forest. *Atmospheric Chemistry and Physics*, 24, 5117–5147. https://doi.org/10.5194/acp-24-5117-2024

Hellén, H., Dommen, J., Metzger, A., Gascho, A., Duplissy, J., Tritscher, T., Prevot, A. S. H., & Baltensperger, U. (2008). Using Proton Transfer Reaction Mass Spectrometry for Online Analysis of Secondary Organic Aerosols. *Environmental Science & Technology*, *42*(19), 7347-7353. https://doi.org/10.1021/es801279m

Hienola, A. I., Pietikäinen, J. P., Jacob, D., Pozdun, R., Petäjä, T., Hyvärinen, A. P., Sogacheva, L., Kerminen, V. M., Kulmala, M., & Laaksonen, A. (2013). Black carbon concentration and deposition estimations in Finland by the regional aerosol–climate model REMO-HAM. *Atmospheric Chemistry and Physics*, *13*(8), 4033-4055. https://doi.org/10.5194/acp-13-4033-2013

Hyvärinen, A. P., Kolmonen, P., Kerminen, V. M., Virkkula, A., Leskinen, A., Komppula, M., Hatakka, J., Burkhart, J., Stohl, A., Aalto, P., Kulmala, M., Lehtinen, K. E. J., Viisanen, Y., & Lihavainen, H. (2011). Aerosol black carbon at five background measurement sites over Finland, a gateway to the Arctic. *Atmospheric Environment*, *45*(24), 4042-4050. https://doi.org/https://doi.org/10.1016/j.atmosenv.2011.04.026

Kendall, M. G.: *Rank correlation methods*, 4th ed., Charles Griffin, London, ISBN 0852641990, 1975.

Kourtchev, I., Giorio, C., Manninen, A., Wilson, E., Mahon, B., Aalto, J., Kajos, M., Venables, D., Ruuskanen, T., Levula, J., Loponen, M., Connors, S., Harris, N., Zhao, D., Kiendler-Scharr, A., Mentel, T., Rudich, Y., Hallquist, M., Doussin, J.-F., . . . Kalberer, M. (2016). Enhanced Volatile Organic Compounds emissions and organic aerosol mass increase the oligomer content of atmospheric aerosols. *Scientific Reports*, *6*(1), 35038. https://doi.org/10.1038/srep35038

Kukkonen, J., López-Aparicio, S., Segersson, D., Geels, C., Kangas, L., Kauhaniemi, M., Maragkidou, A., Jensen, A., Assmuth, T., Karppinen, A., Sofiev, M., Hellén, H., Riikonen, K., Nikmo, J., Kousa, A., Niemi, J. V., Karvosenoja, N., Sousa Santos, G., Sundvor, I., . . . Brandt, J. (2020). The influence of residential wood combustion on the concentrations of PM2.5 in four Nordic cities. *Atmospheric Chemistry and Physics*, *20*(7), 4333-4365. https://doi.org/10.5194/acp-20-4333-2020

Kulmala, M., Hämeri, K., Aalto, P. P., Mäkelä, J. M., Pirjola, L., Douglas Nilsson, E., Buzorius, G., Rannik, Ü., Dal Maso, M., Seidl, W., Hoffman, T., Janson, R., Hansson, H. C., Viisanen, Y., Laaksonen, A., & O'Dowd, C. D.

(2001). Overview of the international project on biogenic aerosol formation in the boreal forest (BIOFOR). *Tellus, Series B: Chemical and Physical Meteorology*, *53*(4), 324-343. https://doi.org/10.3402/tellusb.v53i4.16601

Laakso, L., Grönholm, T., Rannik, Ü., Kosmale, M., Fiedler, V., Vehkamäki, H., & Kulmala, M. (2003). Ultrafine particle scavenging coefficients calculated from 6 years field measurements. *Atmospheric Environment*, *37*(25), 3605-3613. https://doi.org/https://doi.org/10.1016/S1352-2310(03)00326-1

Lack, D. A., & Cappa, C. D. (2010). Impact of brown and clear carbon on light absorption enhancement, single scatter albedo and absorption wavelength dependence of black carbon. *Atmos. Chem. Phys.*, *10*(9), 4207-4220. https://doi.org/10.5194/acp-10-4207-2010

Laing, J. R., Jaffe, D. A., & Hee, J. R. (2016). Physical and optical properties of aged biomass burning aerosol from wildfires in Siberia and the Western USA at the Mt. Bachelor Observatory. *Atmos. Chem. Phys.*, *16*(23), 15185-15197. https://doi.org/10.5194/acp-16-15185-2016

Laj, P., Myhre, C. L., Riffault, V., Amiridis, V., Fuchs, H., Eleftheriadis, K., Petäjä, T., Salameh, T., Kivekäs, N., Juurola, E., Saponaro, G., Philippin, S., Cornacchia, C., Arboledas, L. A., Baars, H., Claude, A., De Mazière, M., Dils, B., Dufresne, M., . . . Vana, M. (2024). Aerosol, Clouds and Trace Gases Research Infrastructure (ACTRIS): The European Research Infrastructure Supporting Atmospheric Science. *Bulletin of the American Meteorological Society*, *105*(7), E1098-E1136. https://doi.org/10.1175/BAMS-D-23-0064.1

Laskin, A., Iedema, M. J., Ichkovich, A., Graber, E. R., Taraniuk, I., & Rudich, Y. (2005). Direct observation of completely processed calcium carbonate dust particles [10.1039/B417366J]. *Faraday Discussions*, *130*(0), 453-468. https://doi.org/10.1039/B417366J

Latimer, R. N. C., & Martin, R. V. (2019). Interpretation of measured aerosol mass scattering efficiency over North America using a chemical transport model. *Atmospheric Chemistry and Physics*, *19*(4), 2635-2653. https://doi.org/10.5194/acp-19-2635-2019

Leskinen, A., Arola, A., Komppula, M., Portin, H., Tiitta, P., Miettinen, P., Romakkaniemi, S., Laaksonen, A., & Lehtinen, K. E. J. (2012). Seasonal cycle and source analyses of aerosol optical properties in a semi-urban environment at Puijo station in Eastern Finland. *Atmospheric Chemistry and Physics*, *12*(12), 5647-5659. https://doi.org/10.5194/acp-12-5647-2012

Lihavainen, H., Hyvärinen, A., Asmi, E., Hatakka, J., & Viisanen, Y. (2015). Long-term variability of aerosol optical properties in northern Finland. *Boreal Environment Research*, *20*(4), 526-541. https://helda.helsinki.fi/items/c1bd369b-1a8d-4646-81b3-66e1c25a2297

Liousse, C., Cachier, H., & Jennings, S. G. (1993). Optical and thermal measurements of black carbon aerosol content in different environments: Variation of the specific attenuation cross-section, σ. *Atmospheric Environment. Part A. General Topics*, *27*(8), 1203–1211. https://doi.org/10.1016/0960-1686(93)90246-U

Luoma, K., Virkkula, A., Aalto, P., Lehtipalo, K., Petäjä, T., & Kulmala, M. (2021). Effects of different correction algorithms on absorption coefficient – a comparison of three optical absorption photometers at a boreal forest site. *Atmos. Meas. Tech.*, *14*(10), 6419-6441. https://doi.org/10.5194/amt-14-6419-2021

Luoma, K., Virkkula, A., Aalto, P., Petäjä, T., & Kulmala, M. (2019). Over a 10-year record of aerosol optical properties at SMEAR II. *Atmospheric Chemistry and Physics*, *19*(17), 11363-11382. https://doi.org/10.5194/acp-19-11363-2019

Magee Scientific, & Aerosol d.o.o. (2018). Aethalometer® Model AE33 user manual (Version 1.56, August 2018). https://home.iiserb.ac.in/~ramyasr/files/Manuals/Manual%20for%20AE33%20%28Aethalometer%29.pdf

Mahowald, N., Albani, S., Kok, J. F., Engelstaeder, S., Scanza, R., Ward, D. S., & Flanner, M. G. (2014). The size distribution of desert dust aerosols and its impact on the Earth system. *Aeolian Research*, *15*, 53-71. https://doi.org/10.1016/j.aeolia.2013.09.002

Mann, H. B. (1945). Nonparametric tests against trend. *Econometrica*, *13*(3), 245–259. https://doi.org/10.2307/1907187

Manninen, H. E., Bäck, J., Sihto-Nissilä, S.-L., Huffman, J. A., Pessi, A.-M., Hiltunen, V., Aalto, P. P., Hidalgo, P. J., Hari, P., Saarto, A., Kulmala, M., & Petäjä, T. (2014). Patterns in airborne pollen and other primary biological aerosol particles (PBP), and their contribution to aerosol mass and number in a boreal forest. *Boreal Environment Research*, *19*, 383-405. https://helda.helsinki.fi/server/api/core/bitstreams/f1408a0d-26ad-4b3d-91bc-db8b0e8e603a/content

Maso, M. D., Kulmala, M., Riipinen, I., Wagner, R., Hussein, T., Aalto, P. P., & Lehtinen, K. E. J. (2005). Formation and growth of fresh atmospheric aerosols: eight years of aerosol size distribution data from SMEAR II, Hyytiälä, Finland. *Boreal Environment Research*, *10*, 323–336.

McFiggans, G., Artaxo, P., Baltensperger, U., Coe, H., Facchini, M. C., Feingold, G., Fuzzi, S., Gysel, M., Laaksonen, A., Lohmann, U., Mentel, T. F., Murphy, D. M., O'Dowd, C. D., Snider, J. R., & Weingartner, E. (2006). The effect of physical and chemical aerosol properties on warm cloud droplet activation. *Atmos. Chem. Phys.*, *6*(9), 2593-2649. https://doi.org/10.5194/acp-6-2593-2006

Moosmüller, H., Chakrabarty, R. K., & Arnott, W. P. (2009). Aerosol light absorption and its measurement: A review. *Journal of Quantitative Spectroscopy and Radiative Transfer*, *110*(11), 844-878. https://doi.org/https://doi.org/10.1016/j.jqsrt.2009.02.035

Müller, T., Henzing, J. S., de Leeuw, G., Wiedensohler, A., Alastuey, A., Angelov, H., Bizjak, M., Collaud Coen, M., Engström, J. E., Gruening, C., Hillamo, R., Hoffer, A., Imre, K., Ivanow, P., Jennings, G., Sun, J. Y., Kalivitis, N., Karlsson, H., Komppula, M., . . . Wang, Y. Q. (2011). Characterization and intercomparison of aerosol absorption photometers: result of two intercomparison workshops. *Atmospheric Measurement Techniques*, *4*(2), 245-268. https://doi.org/10.5194/amt-4-245-2011

Ogren, J. A. (2010). Comment on "Calibration and intercomparison of filter-based measurements of visible light absorption by aerosols". *Aerosol Science and Technology*, 44(8), 589–591. https://doi.org/10.1080/02786826.2010.482111

Pandolfi, M., Alados-Arboledas, L., Alastuey, A., Andrade, M., Angelov, C., Artiñano, B., Backman, J., Baltensperger, U., Bonasoni, P., Bukowiecki, N., Collaud Coen, M., Conil, S., Coz, E., Crenn, V., Dudoitis, V., Ealo, M., Eleftheriadis, K., Favez, O., Fetfatzis, P., . . . Laj, P. (2018). A European aerosol phenomenology – 6:

scattering properties of atmospheric aerosol particles from 28 ACTRIS sites. *Atmos. Chem. Phys.*, *18*(11), 7877-7911. https://doi.org/10.5194/acp-18-7877-2018

Pandolfi, M., Ripoll, A., Querol, X., & Alastuey, A. (2014). Climatology of aerosol optical properties and black carbon mass absorption cross section at a remote high-altitude site in the western Mediterranean Basin. *Atmospheric Chemistry and Physics*, *14*(12), 6443-6460. https://doi.org/10.5194/acp-14-6443-2014

Petäjä, T., Järvi, L., Kerminen, V. M., Ding, A. J., Sun, J. N., Nie, W., Kujansuu, J., Virkkula, A., Yang, X., Fu, C. B., Zilitinkevich, S., & Kulmala, M. (2016). Enhanced air pollution via aerosol-boundary layer feedback in China. *Scientific Reports*, *6*(July 2015), 1-6. https://doi.org/10.1038/srep18998

Petäjä, T., Tabakova, K., Manninen, A., Ezhova, E., O'Connor, E., Moisseev, D., Sinclair, V. A., Backman, J., Levula, J., Luoma, K., Virkkula, A., Paramonov, M., Räty, M., Äijälä, M., Heikkinen, L., Ehn, M., Sipilä, M., Yli-Juuti, T., Virtanen, A., . . . Kerminen, V. M. (2022). Influence of biogenic emissions from boreal forests on aerosol–cloud interactions. *Nature Geoscience*, *15*(1), 42-47. https://doi.org/10.1038/s41561-021-00876-0

Petäjä, T., Ylivinkka, I., Kokkonen, T., Schiestl-Aalto, P., Kerminen, V.-M., Bäck, J., & Kulmala, M. (2025). Chapter 15 - Air quality and the environmental impacts. In R. S. Sokhi (Ed.), *Air Quality* (pp. 439-462). Elsevier. https://doi.org/https://doi.org/10.1016/B978-0-12-822591-2.00015-9

Petzold, A., Schloesser, H., Sheridan, P. J., Arnott, W. P., Ogren, J. A., & Virkkula, A. (2005). Evaluation of multiangle absorption photometry for measuring aerosol light absorption. *Aerosol Science and Technology*, *39*(1), 40-51. https://doi.org/10.1080/027868290901945

Petzold, A., & Schönlinner, M. (2004). Multi-angle absorption photometry - A new method for the measurement of aerosol light absorption and atmospheric black carbon. *Journal of Aerosol Science*, *35*(4), 421-441. https://doi.org/10.1016/j.jaerosci.2003.09.005

Rantala, P., Aalto, J., Taipale, R., Ruuskanen, T. M., & Rinne, J. (2015). Annual cycle of volatile organic compound exchange between a boreal pine forest and the atmosphere. *Biogeosciences*, *12*(19), 5753-5770. https://doi.org/10.5194/bg-12-5753-2015

Saturno, J., Pöhlker, C., Massabò, D., Brito, J., Carbone, S., Cheng, Y., Chi, X., Ditas, F., Hrab De Angelis, I., Morán-Zuloaga, D., Pöhlker, M. L., Rizzo, L. V., Walter, D., Wang, Q., Artaxo, P., Prati, P., & Andreae, M. O. (2017). Comparison of different Aethalometer correction schemes and a reference multi-wavelength absorption technique for ambient aerosol data. *Atmospheric Measurement Techniques*, *10*(8), 2837-2850. https://doi.org/10.5194/amt-10-2837-2017

Schneider, J., Höhler, K., Heikkilä, P., Keskinen, J., Bertozzi, B., Bogert, P., Schorr, T., Umo, N. S., Vogel, F., Brasseur, Z., Wu, Y., Hakala, S., Duplissy, J., Moisseev, D., Kulmala, M., Adams, M. P., Murray, B. J., Korhonen, K., Hao, L., . . . Möhler, O. (2021). The seasonal cycle of ice-nucleating particles linked to the abundance of biogenic aerosol in boreal forests. *Atmospheric Chemistry and Physics*, *21*(5), 3899-3918. https://doi.org/10.5194/acp-21-3899-2021

Schuster, G. L., Dubovik, O., & Holben, B. N. (2006). Angstrom exponent and bimodal aerosol size distributions. *Journal of Geophysical Research Atmospheres*, *111*(7), 1-14. https://doi.org/10.1029/2005JD006328

Seinfeld, J. H., & Pandis, S. N. (2016). *Atmospheric Chemistry and Physics: From Air Pollution to Climate Change*. Wiley. https://books.google.fi/books?id=n_RmCgAAQBAJ

Sen, P. K. (1968). Estimates of the regression coefficient based on Kendall's tau. *Journal of the American Statistical Association*, *63*(324), 1379–1389. https://doi.org/10.1080/01621459.1968.10480934

Sheridan, P. J., & Ogren, J. A. (1999). Observations of the vertical and regional variability of aerosol optical properties over central and eastern North America. *Journal of Geophysical Research Atmospheres*, *104*(D14), 16793-16805. https://doi.org/10.1029/1999JD900241

Smith, S. J., Van Aardenne, J., Klimont, Z., Andres, R. J., Volke, A., & Delgado Arias, S. (2011). Anthropogenic sulfur dioxide emissions: 1850-2005. *Atmospheric Chemistry and Physics*, *11*(3), 1101-1116. https://doi.org/10.5194/acp-11-1101-2011

Theil, H. (1950). A rank-invariant method of linear and polynomial regression analysis. *Proceedings of the Royal Netherlands Academy of Sciences*, *53*, 386–392, 521–525, 1397–1412. https://dwc.knaw.nl/DL/publications/PU00018789.pdf

Tian, P., Yu, Z., Cui, C., Huang, J., Kang, C., Shi, J., Cao, X., & Zhang, L. (2023). Atmospheric aerosol size distribution impacts radiative effects over the Himalayas via modulating aerosol single-scattering albedo. *npj Climate and Atmospheric Science*, *6*(1). https://doi.org/10.1038/s41612-023-00368-5

Titos, G., Burgos, M. A., Zieger, P., Alados-Arboledas, L., Baltensperger, U., Jefferson, A., Sherman, J., Weingartner, E., Henzing, B., Luoma, K., O'Dowd, C., Wiedensohler, A., & Andrews, E. (2021). A global study of hygroscopicity-driven light-scattering enhancement in the context of other in situ aerosol optical properties. *Atmospheric Chemistry and Physics*, *21*(17), 13031-13050. https://doi.org/10.5194/acp-21-13031-2021

Tørseth, K., Aas, W., Breivik, K., Fjæraa, A. M., Fiebig, M., Hjellbrekke, A. G., Lund Myhre, C., Solberg, S., & Yttri, K. E. (2012). Introduction to the European Monitoring and Evaluation Programme (EMEP) and observed atmospheric composition change during 1972–2009. *Atmos. Chem. Phys.*, *12*(12), 5447-5481. https://doi.org/10.5194/acp-12-5447-2012

Tunved, P., Hansson, H. C., Kerminen, V. M., Ström, J., Dal Maso, M., Lihavainen, H., Viisanen, Y., Aalto, P. P., Komppula, M., & Kulmala, M. (2006). High natural aerosol loading over boreal forests. *Science*, *312*(5771), 261-263. https://doi.org/10.1126/science.1123052

van de Hulst, H. C.: *Multiple light scattering: Tables, formulas, and applications*, Vol. 1, Academic Press, New York, 1980. https://www.sciencedirect.com/book/9780127107011/multiple-light-scattering

Varga, G., Meinander, O., Rostási, Á., Dagsson-Waldhauserova, P., Csávics, A., & Gresina, F. (2023). Saharan, Aral-Caspian and Middle East dust travels to Finland (1980–2022). *Environment International*, *180*(September). https://doi.org/10.1016/j.envint.2023.108243

Virkkula, A. (2010). Correction of the calibration of the 3-wavelength Particle Soot Absorption Photometer (3λ PSAP). *Aerosol Science and Technology*, 44(8), 706–712. https://doi.org/10.1080/02786826.2010.482110

Virkkula, A., Mäkelä, T., Hillamo, R., Yli-Tuomi, T., Hirsikko, A., Hämeri, K., & Koponen, I. K. (2007). A simple procedure for correcting loading effects of aethalometer data. *Journal of the Air & Waste Management Association*, *57*(10), 1214–1222. https://doi.org/10.3155/1047-3289.57.10.1214

Virkkula, A., Backman, J., Aalto, P. P., Hulkkonen, M., Riuttanen, L., Nieminen, T., Dal Maso, M., Sogacheva, L., De Leeuw, G., & Kulmala, M. (2011). Seasonal cycle, size dependencies, and source analyses of aerosol optical properties at the SMEAR II measurement station in Hyytiälä, Finland. *Atmospheric Chemistry and Physics*, *11*(9), 4445-4468. https://doi.org/10.5194/acp-11-4445-2011

Weingartner, E., Saathoff, H., Schnaiter, M., Streit, N., Bitnar, B., & Baltensperger, U. (2003). Absorption of light by soot particles: Determination of the absorption coefficient by means of aethalometers. *Journal of Aerosol Science*, *34*(10), 1445-1463. https://doi.org/10.1016/S0021-8502(03)00359-8

Yli-Panula, E., Fekedulegn, D. B., Green, B. J., & Ranta, H. (2009). Analysis of airborne Betula pollen in Finland: a 31-year perspective. *International Journal of Environmental Research and Public Health*, *6*(6), 1706-1723. https://doi.org/10.3390/ijerph6061706

Yttri, K. E., Canonaco, F., Eckhardt, S., Evangeliou, N., Fiebig, M., Gundersen, H., Hjellbrekke, A.-G., Lund Myhre, C., Platt, S. M., Prévôt, A. S. H., Simpson, D., Solberg, S., Surratt, J., Tørseth, K., Uggerud, H., Vadset, M., Wan, X., & Aas, W. (2021). Trends, composition, and sources of carbonaceous aerosol at the Birkenes Observatory, northern Europe, 2001–2018. *Atmospheric Chemistry and Physics*, *21*(9), 7149-7170. https://doi.org/10.5194/acp-21-7149-2021

Yue, S., & Wang, C. Y. (2004). The Mann–Kendall test modified by effective sample size to detect trend in serially correlated hydrological series. *Water Resources Management*, *18*(3), 201–218. https://doi.org/10.1023/B:WARM.0000043140.61082.60

Yus-Díez, J., Bernardoni, V., Močnik, G., Alastuey, A., Ciniglia, D., Ivančič, M., Querol, X., Perez, N., Reche, C., Rigler, M., Vecchi, R., Valentini, S., & Pandolfi, M. (2021). Determination of the multiple-scattering correction factor and its cross-sensitivity to scattering and wavelength dependence for different AE33 Aethalometer filter tapes: a multi-instrumental approach. *Atmospheric Measurement Techniques*, *14*(10), 6335-6355. https://doi.org/10.5194/amt-14-6335-2021

Zhang, L., Gong, S., Padro, J., & Barrie, L. (2001). A size-segregated particle dry deposition scheme for an atmospheric aerosol module. *Atmospheric Environment*, *35*(3), 549-560. https://doi.org/https://doi.org/10.1016/S1352-2310(00)00326-5

Zieger, P., Aalto, P. P., Aaltonen, V., Äijälä, M., Backman, J., Hong, J., Komppula, M., Krejci, R., Laborde, M., Lampilahti, J., De Leeuw, G., Pfüller, A., Rosati, B., Tesche, M., Tunved, P., Väänänen, R., & Petäjä, T. (2015). Low hygroscopic scattering enhancement of boreal aerosol and the implications for a columnar optical closure study. *Atmospheric Chemistry and Physics*, *15*(13), 7247-7267. https://doi.org/10.5194/acp-15-7247-2015

Formatted: Indent: Left: -0.06"

Formatted: Font: Font color: Text 1, English (United States), Do not check spelling or grammar

Zieger, P., Fierz-Schmidhauser, R., Gysel, M., Ström, J., Henne, S., Yttri, K. E., Baltensperger, U., & Weingartner, E. (2010). Effects of relative humidity on aerosol light scattering in the Arctic. *Atmos. Chem. Phys.*, *10*(8), 3875-3890. https://doi.org/10.5194/acp-10-3875-2010

Zotter, P., Herich, H., Gysel, M., El-Haddad, I., Zhang, Y., Mocnik, G., Hüglin, C., Baltensperger, U., Szidat, S., & Prévôt, A. S. H. (2017). Evaluation of the absorption Ångström exponents for traffic and wood burning in the Aethalometer-based source apportionment using radiocarbon measurements of ambient aerosol. *Atmospheric Chemistry and Physics*, *17*(6), 4229-4249. https://doi.org/10.5194/acp-17-4229-2017